THE HONG KONG
POLYTECHNIC UNIVERSITY
香港理工大學
Pao Yue-kong Library
包玉剛圖書館

Copyright Undertaking

This thesis is protected by copyright, with all rights reserved.

By reading and using the thesis, the reader understands and agrees to the following terms:

1. The reader will abide by the rules and legal ordinances governing copyright regarding the use of the thesis.

2. The reader will use the thesis for the purpose of research or private study only and not for distribution or further reproduction or any other purpose.

3. The reader agrees to indemnify and hold the University harmless from and against any loss, damage, cost, liability or expenses arising from copyright infringement or unauthorized usage.

Pao Yue-kong Library, The Hong Kong Polytechnic University, Hung Hom, Kowloon, Hong Kong

http://www.lib.polyu.edu.hk

ADVANCED TEXTILE IMAGE ANALYSIS BASED ON MULTISPECTRAL

COLOUR REPRODUCTION

YAO PENGPENG

PhD

The Hong Kong Polytechnic University

2022

The Hong Kong Polytechnic University

Institute of Textiles and Clothing

Advanced textile image analysis based on multispectral colour reproduction

Yao Pengpeng

A thesis submitted in partial fulfilment of the requirements for the degree of Doctor of

Philosophy

September 2021

CERTIFICATE OF ORIGINALITY

I hereby declare that this thesis is my own work and that, to the best of my knowledge and belief, it reproduces no material previously published or written, nor material that has been accepted for the award of any other degree or diploma, except where due acknowledgement has been made in the text.

_____ (Signed)

_____Yao Pengpeng_____(Name of student)

Abstract

In this study, multispectral colour reproduction methods are investigated using textile images. Accurate colour reproduction of textile is crucial for the industry in terms of colour communication, colour measurement and quality control. Traditional colour measurement and colour communication are usually performed by spectrophotometers. The disadvantages of using spectrophotometers are that (1) they only measure a small area of the fabric at a time and (2) they lack the spatial reflectance information of the fabric.

The contribution of this thesis can be listed as follows:

(1) Proposed an improved reflectance reconstruction method based on L1-norm penalization. Spectral reflectance reconstruction for multispectral images (such as Weiner estimation) may perform sub-optimally when the object being measured has a texture that is not in the training set. The accuracy of reconstruction is significantly lowered without training samples. Using L1-norm, our method can provide the transformation matrix with the favorable sparse property, which can help to achieve better results when measuring the unseen samples. We verify the proposed method by reconstructing spectral reflection for 4 types of materials (cotton, paper, polyester, and nylon) captured by a multi-spectral imaging system. Each of the materials has its own texture and there are 204 samples in each of the materials / textures in the experiments. Experimental results show that when the texture is not included in the training dataset, L1-norm can achieve better results compared with existing methods using colourimetric measure (i.e., colour difference) and shows consistent accuracy across 4 kinds of materials.

(2) Achieved accurate whiteness measurement in textile with the presence of fluorescent whitening agents (FWAs). Accurate whiteness measurement is important in many industries such as textile, paper and detergent production. With the advent of FWAs over the past decades, the general idea of whiteness has been changed from measuring reflectance to determining the spectral radiance factor (SRF) of the materials. Multispectral Imaging (MSI) system has long been investigated and is known to be an advanced technique to measure the reflectance of objects, by which one can use it to accurately measure the colour of objects. However, the spectral surface will be heavily augmented by the fluorescent materials added to the objects. As a result, measuring whiteness does not only depend on reflectance measurement but also SRF measurement. A specialized light-source is designed with an ultraviolet (UV) filter to control and adjust the illumination system in an integrating sphere. Through the adjustment of the position of the UV filter, multispectral images of an object (fabric in this work) are captured with different exposures of UV light from the light-source. Then these images are processed and combined by our proposed method into a new multispectral image with full-range visible spectral information. Besides, based on a theoretical proof, this work shows that MSI is spatial uniform for SRF measurement. Through the custom light-source with an adjustable UV filter, whiteness metric that is comparable with a spectrophotometer can be obtained by MSI. This work shows that MSI can achieve high whiteness measurement accuracy and spatial uniformity.

(3) Implemented a new clustering algorithm for measuring colours and recognizing patterns in printed fabrics. There are rich colours and various patterns with different sizes and shapes in printed fabrics, which make it difficult for accurate colour measurement and pattern recognition by traditional spectrophotometer and digital camera. This work proposes a grid-based density peaks clustering (GDPC) algorithm

to measure colours and recognize patterns of multispectral image of printed fabrics. A custom-developed multispectral imaging system is used to capture the multispectral fabric image where each pixel has full spectral information across the visible spectrum from 400 nm to 700 nm with an interval of 10 nm. The multispectral image is then converted to CIELAB colour space for image processing (clustering) and colour measurement. The noise pixels are removed by calculating the local stability of each pixel, and then the remaining pixels are clustered by the proposed grid-based density peaks clustering algorithm based on the CIELAB colour values. Experiment results show that, when compared with conventional colour clustering algorithms, the proposed GDPC algorithm can have higher accuracy and efficiency in colour separation from multispectral images with complex patterns.

(4) Proposed a new approach to classify knitted fabrics. Automatic inspection of fabrics has tremendous advantage over the manual inspection due to its' great efficiency. Based on BoW (Bag of Word) feature extraction, a new approach for classification of knitted stitch was proposed. By this method, the classification of knitted fabrics can be significantly improved. To validate the method, we fabricated 58 texture knitted fabrics with 5 colours. The result shows our method can reach the best classification accuracy. This work will benefit the research of automatic recognition of textile pattern.

Overall, this work has improved the technical aspects in fabric industry using advanced computational methods.

List of Publications

The following journal and conference papers have been published based on the results generated from this work.

Journal Paper

Spectral reflectance reconstruction using L1-norm penalization for colour reproduction (Submitted to ***Applied Optics***)

Florescent whiteness measurement by multispectral imaging system (In preparation)

Automatic classification of knitted fabric textile based on Bag-Of-Words (BoW) and K-Nearest-Neighbor (KNN) Algorithms (In preparation)

Automatic color pattern recognition of multicolor printed fabrics using multispectral image system (In processing)

Conference paper

Wu, Hochung, **Yao, Pengpeng**., Shao, S. J., and Xin, J. H. An empirical study on fabric image retrieval using colour and pattern. *Progress in Colour Studies 2018*

Yao, Pengpeng, and John H. Xin. "KNITTED FABRIC TEXTILE CLASSIFICATION BASED ON GLOBAL FEATURE." *Proceedings of the 19th World Textile Conference-Autex 2019*. 2019.

Yao, Pengpeng, Hochung, Wu, and John H. Xin "The use of LED-based illumination for Multispectral Imaging System" International Color Association (AIC), 2021.

Book Chapter

Xin, J., Wu, J., **Yao, P**., & Shao, S. (2018). An empirical study on fabric image retrieval with multispectral images using colour and pattern features. *Progress in Colour Studies: Cognition, language and beyond*, 391.

Acknowledgements

I would like to take this opportunity to express the people who cared about me and helped me during my five-year Ph.D career.

First, I want to thank my mentor, Prof John Xin, who is gentle, strong, knowledgeable and humble, and has always guided me. Without the Ph.D opportunity he gave, there would be no where I am today.

Then I thank the friends in my laboratory, it is you who have given me enough support in academic and daily life. They are Dr. Ma Kaikai, Fan Suju, Xia gang.

Again, I thank my friend Jack HoChung Wu, without your help, hardly can I think I will end my Ph.D degree. Thank for Yadie Yang, Jiali Yu, QiuQiong Shi. Thank for friends in Peking University, there are Zhipeng Mo, Hao Zhang. Thank you for friends in Zhejiang University, they are Quangeng Ge, Ze Zou and Yu Gao.

Finally, I thank my parents and my sister.

Table of content

Contents

Nomenclature

List of Abbreviations

BoF	Bag of Feature
BoW	Bag of Word
CBIR	Content Based Image Retrieval
CIE	International Commission on Illumination
CMC	Color Measurement Committee
CPU	Central Processing Unit
FCM	Fuzzy C-means Clustering
FWA	Fluorescent Whitening Agent
HSI	Hyperspectral imaging
ICM	Imaging Colour Measurement
ISO	International Organization for Standardization
MSI	Multispectral imaging
PC	Personal Computer
RAM	Random Access Memory
SIFT	Scale Invariant Feature Transform
std	Standard deviation
SURF	Speeded Up Robust Features
UV	Ultraviolet

Chapter 1 Introduction

1.1 Introduction to textile image analysis and multispectral imaging

This chapter first introduces the background of textile image analysis and multispectral imaging. The objective and main contribution of this work are addressed. Finally, a general outline of the overall structure of this thesis is presented.

Accurate colour reproduction of image can facilitate the process of colour communication, colour measurement and quality control (Herzog & Hill, 2003). One of the most important topics of this work is focused on the colour and whiteness measurement.

Colour and whiteness measurements have always been very important aspects for many industries like textile, paper and detergent production (McDonald, 1997; Uchida, 1998). For example, a large batch of fabric samples with inconsistent colour would be rejected by a client which could incur negative financial impacts on the fabric manufacturer. There are currently two main categories of instrument for measuring spectral reflectance accurately, i.e., spectrophotometers and multispectral imaging systems. Spectrophotometers, like DataColor 650 and X-Rite Ci7860, have proven to be very effective in measuring colour and they are used as standard instrument in industries. However, the limitation in using spectrophotometers is that one can only measure the average reflectance of an area without any spatial resolution. Moreover, spectrophotometers cannot measure small objects such as a yarn (Luo, Shao, Shen, & Xin, 2013).

On the other hand, multispectral imaging technology has shown enormous potential in colour measurement because it can provide spectral information as well as spatial information (Westland, Ripamonti, & Cheung, 2012). Another advantage of multispectral colour measurement is that, by various image processing and machine learning technologies, the colour of a very small object or area such as a yarn can be measured.

In the recent years, the advent of Fluorescent whitening agents (FWA) has changed the measurement of whiteness (Puebla, 2006b). Fluorescent molecules have the property to absorb light in the near ultra-violet (UV) wavelength (i.e., below 400nm) and emit light at about 445 nm (Puebla, 2006b). Many spectrophotometers (e.g., DataColor 650 and X-rite Ci7860) can measure the surface with FWAs by different methods, such as one-point-matching and numerical method (Yang, 2017). However, to the best of our knowledge, there are no report about the measurement of whiteness by multispectral imaging technology in the literature. In this study, we propose to use a special multispectral imaging machine to measure the whiteness. A crucial part in whiteness measurement is whiteness calibration because the whiteness is highly depended on the spectral distribution of light source. A new method for whiteness calibration and whiteness measurement is developed in this study, which, from the experimental results, achieved high accuracy.

Multispectral imaging system has been tested to be a very efficient method in textile image acquisition. Having the described applications in mind, certain aspects influence the design of a multispectral imaging system.

1.2 Research Background

Textile image processing has been an important part of image processing since 1960 (L. Luo, H. L. Shen, S. J. Shao, & J. H. Xin, 2015b). With the image processing method, more and more tasks can be done. Imaging capture devices basically consist of an optoelectronic sensor, or analogical photosensor, and a device which converts analogical signals into a digital code. Spatial uniformity is very important feature in colour measurement.

In many cases where the accuracy of a colour is a major quality criterion, companies do not relay on colour measurement, but make use of visual assessments. Traditional colour measurement and communication are based on spectrophotometers. Spectrophotometers are the most widely used instruments to measure instrumental colours pf fabric samples in textile and garment industries. A spectrophotometer can provide accurate and precise spectral resolution for fabric samples. The spectral reflectance is independent of characteristics of acquisition systems and illuminates, i.e., the measurement results of a spectrophotometer can be transformed to any colour space and can be interpreted for any other illuminates. However, there are three limitations when spectrophotometers are employed to measure colours of textiles.

1.3 Research objectives

This project will investigate into the theory of textile image analysis and its' application.

1. To develop a spectral reflectance reconstruction method. Traditional multispectral system usually using Weiner estimation for reflectance reconstruction perform sub-optimally when the object being measured has a texture that is not in the training set.

2. To develop fluorescent whiteness measurement part by using multispectral system. Different from general colour metric, fluorescent whiteness does not depend on spectral reflectance but on total radiance because fluorescence agents absorb light in UV region and emit energy in visual wavelength.

3. To investigate and apply appropriate computational technologies to analyze fabric images. Fabric classification and pattern detection are important procedures which can be benefited from the automatic process enabled by computer algorithms.

1.4 Research Significance and Value

This project will greatly contribute to the textile and computing vision. The study contributes to the literature on textile colour measurement, quality control, colour communication, colour management, image processing and retrieval. The outcome of this study would make a significant contribution to colour measurement of yarn dyed fabrics. The details are as follows.

(1) Proposed an improved reflectance reconstruction method based on L1-norm penalization. Spectral reflectance reconstruction for multispectral images (such as Weiner estimation) may perform sub-optimally when the object being measured has a texture that is not in the training set. The accuracy of reconstruction is significantly lower without training samples. Using L1-norm, our method can provide the transformation matrix with the favourable sparse property, which can help to achieve better results when measuring the unseen samples. We verify the proposed method by reconstructing spectral reflection for 4 types of materials (cotton, paper, polyester, and nylon) captured by a multi-spectral imaging system. Each of the materials has its own texture and there are 204 samples in each of the materials / textures in the experiments.

Experimental results show that when the texture is not included in the training dataset, L1-norm can achieve better results compared with existing methods using colourimetric measure (i.e., colour difference) and shows consistent accuracy across 4 kinds of materials.

(2) Achieved accurate whiteness measurement in textile with the presence of fluorescent whitening agents (FWAs). Accurate whiteness measurement is important in many industries such as textile, paper and detergent production. With the advent of fluorescent whitening agents (FWAs) over the past decades, the general idea of whiteness has been changed from measuring reflectance to determining the spectral radiance factor (SRF) of the materials. Multispectral Imaging (MSI) system has long been investigated and is known to be an advanced technique to measure the reflectance of objects, by which one can use it to accurately measure the colour of objects. However, the spectral surface will be heavily augmented by the fluorescent materials added to the objects. As a result, measuring whiteness does not only depend on reflectance measurement but also SRF measurement. In this paper, a specialized light-source is designed with an ultraviolet (UV) filter to control and adjust the illumination system in an integrating sphere. Through the adjustment of the position of the UV filter, multispectral images of an object (fabric in this work) are captured with different exposures of UV light from the light-source. Then these images are processed and combined by our proposed method into a new multispectral image with full-range visible spectral information. Besides, based on a theoretical proof, this work shows that MSI is spatial uniform for SRF measurement. Through the custom light-source with an adjustable UV filter, whiteness metric that is comparable with a spectrophotometer can be obtained by MSI. This work shows that MSI can achieve high whiteness measurement accuracy and spatial uniformity.

(3) Implemented a new clustering algorithm for measuring colours and recognizing patterns in printed fabrics. There are rich colours and various patterns with different

5

sizes and shapes in printed fabrics, which make it difficult for accurate colour measurement and pattern recognition by traditional spectrophotometer and digital camera. This work proposes a grid-based density peaks clustering (GDPC) algorithm to measure colours and recognize patterns of multispectral image of printed fabrics. A custom-developed multispectral imaging system is used to capture the multispectral fabric image where each pixel has full spectral information across the visible spectrum from 400 nm to 700 nm with an interval of 10 nm. The multispectral image is then converted to CIELAB colour space for image processing (clustering) and colour measurement. The noise pixels are removed by calculating the local stability of each pixel, and then the remaining pixels are clustered by the proposed grid-based density peaks clustering algorithm based on the CIELAB colour values. Experiment results show that, when compared with conventional colour clustering algorithms, the proposed GDPC algorithm can have higher accuracy and efficiency in colour separation from multispectral images with complex patterns.

(4) Proposed a new approach to classify knitted fabrics. Automatic inspection of fabrics has tremendous advantage over the manual inspection due to its' great efficiency. In this paper, based on BoW (Bag of Word) feature extraction, a new approach for classification of knitted stitch was proposed. By this method, the classification of knitted fabrics can be significantly improved. To validate the method, we fabricated 58 texture knitted fabrics with 5 colour. The result shows our method can reach the best. This work will benefit the research of automatic recognition of textile pattern.

1.5 Outline of the Work

There are seven chapters in this report. Chapter 1 mainly focuses on the background of this research, as well as the main problems in the current field and the objectives of this research. A literature review is provided in Chapter 2, which includes a review on multispectral imaging for colour measurement and its applications. Chapter 3 focuses on reflectance reconstruction. Chapter 4 describes our proposed method for whiteness measurement using multispectral imaging system. Chapter 5 reports the results of automatic classification of knitted fabrics. Chapter 6 introduces the textile image processing methods in printing fabric colour patten recognition. The last chapter (Chapter 7)concludes the thesis and discusses the plans of further work.

Chapter 2 Literature Review

2.1 Introduction

A detailed literature survey is given in this chapter to provide the background information related to faithful colour reproduction of image. The related work is reviewed from two perspectives: multispectral imaging theory and its applications. Multispectral imaging theory refers to the hardware and software of multispectral imaging system while the applications of multispectral imaging system include colour measurement, wetness measurement, florescence separation and so on.

2.2 Multispectral Image Theory

There are multiple methods for capturing multispectral images, including filter wheel-based MSI, LCTF based MSI, scan-push hyperspectral imaging system. The methods are discussed in this section together with the corresponding advantages and disadvantages.

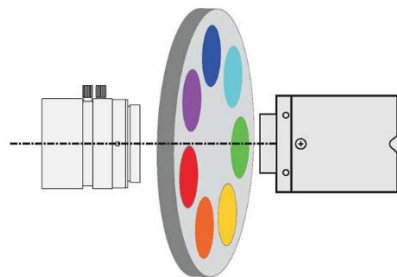### 2.2.1 Multispectral imaging by filter wheel

Figure 2.1 Filter wheel for multispectral imaging

As it's shown in the image, the camera is combined by a lens, filter wheel and a camera. This has been well investigated by Johannes and Til (Brauers & Aach, 2011; Brauers & Aach, 2010; Brauers, Schulte, & Aach, 2008; Chen, Shen, Li, & Xin, 2017; Chen & Shen, 2015; Shrestha & Hardeberg, 2014). When the wheel turns to a channel, the monochrome camera will take a photo. As a result, the number of channels will be the dimension of the multispectral imaging system. For example, if there are 10 filters on the wheel, the acquired multispectral images will be a 10-channel image that different from the grey images (one channel) and RGB image (three channels).

2.2.2 Multispectral imaging by LCTF

Liquid crystal tunable filters (LCTFs) is similar to filter wheel as it can change the filters by programming. (Martínez-Domingo et al., 2017; Tominaga & Okajima, 2000) The LCTFs have obvious advantage over filter wheel that they can be much faster without the physical move of wheels. However, they also have the disadvantages of imbalanced transfer rate especially towards the violate region. Figure 2.2 shows the difference between a filter wheel and LCTFs. One can observe that the transmission rate from 400-450nm is very small. Because of this, many previous research works have adopted the filter wheel as their device. LCTF are widely used in the real time required imaging environment like medicine imaging.
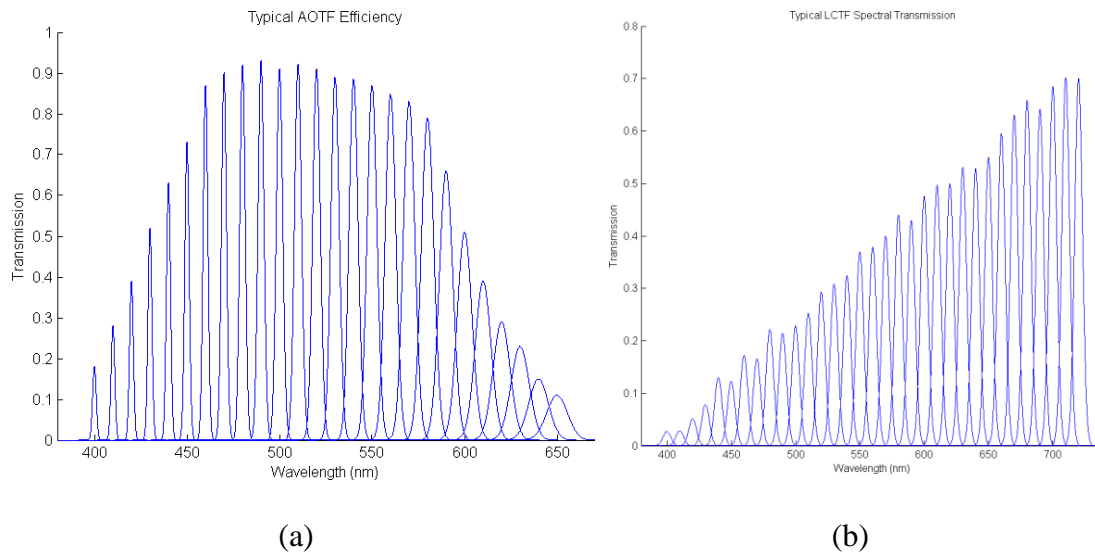
Figure 2.2 (a): Typical transmission as a function of wavelength for a ordinary optic tunable filter; (b): Typical transmission for a liquid crystal tunable filter.

Colour measurement by multispectral imaging is highly related with reflectance reconstruction or spectral reconstruction(Ying Fu, Lam, Sato, Okabe, & Sato, 2013), since the resultant colour is dependent on the spectral reflectance (Westland et al., 2012).

Fluorescence imaging by multispectral imaging technology has been widely researched recently(Ying Fu et al., 2013; Sato, Okabe, & Sato, 2012; C. Zhang & Sato, 2013; Zheng, Sato, & Sato, 2014), and that has paved the path for this study to measure the whiteness of the FWAs added white fabric. Fluorescence material has a special property that absorb energy in lower band and reemit it in higher band, namely Stroke Shift, which in colour science, will make colour more vivid in that wavelength(Ying Fu et al., 2013).

The review of the commercial multispectral system can be summarized in Table 2.1.

Table 2.1 Review of different multispectral imaging system

	Number of bans	Spectral range	advantage	disadvantage
LCTF	31	420-700 nm	fast	Transmission rate
Filter-wheel	16	400-700 nm	slow	excellent
Push-scan hyperspectral	96	400-1000 nm	slow	excellent
LED hyperspectral	16		fast	Unacceptable in short wavelength

2.3 Multispectral Image Application

2.3.1 Multispectral Imaging In textile industry

Luo et al. (L. Luo, H. L. Shen, S. J. Shao, & J. Xin, 2015a; L. Luo, H. L. Shen, S. J. Shao, & J. H. Xin, 2015c; Luo, Shen, Shao, & Xin, 2016) have developed significant amount of works to apply the multispectral imaging technology in textile industry.

2.3.2 Multispectral Imaging for Florescence

Recently, multispectral imaging technology has been widely used in Florence appearance revolver. Different from traditional material, it follows the Stork theory which means that the material absorb energy from the short wavelength and emit at the longer wavelength, which means the radiance not only depend on the material but also depend on the power of illumination.

Fu et al.(Y. Fu, Lam, Kobashi, et al., 2014; Y. Fu, Lam, Matsushita, Sato, & Sato, 2014; Y. Fu et al., 2013; Y. Fu, Zheng, Zhang, & Huang, 2018) proposed to use conventional RGB camera and varied coloured illuminations to recover the reflectance and fluorescence spectral information. They exploit the illuminant-invariant chromaticity of fluorescence to estimate both spectral reflectance and fluorescent chromaticity from RGB images.

Tominaga et al. (Hirai, Osawa, Hori, Horiuchi, & Tominaga, 2018; Tominaga, Hirai, & Horiuchi, 2018a, 2018b, 2019; Tominaga & Okajima, 2000) use multispectral imaging technology (mainly LCTF) to recover the spectral data of a florescent objects. Different from Fu et al. metioned above, Tominaga recover both the reflectance and the absorb and emission matrix at the same time.

2.3.3 Multispectral Imaging for wetness

Shimano (Okawa et al., 2019; M. Shimano et al., 2017) developed an algorithm for wetness detection by multispectral imaging. This research shows that colour change, particularly in its spectral behaviour, carries rich information about a wet surface. They derive an analytical spectral appearance model of wet surfaces that expresses the characteristic spectral sharpening due to multiple scattering and absorption in the surface.

2.4 Multispectral imaging employed in this study

In this section, the customized MSI and the reflectance reconstruction

method will be introduce.

2.4.1 Customized MSI employed

A MSI 16-channel filter-wheel MSI system is developed to accomplish this thesis called Imaging Colour Measurement (ICM). Before capturing the multispectral data, ICM need to be calibrated. This calibration process comprises exposure time estimation, illumination balance, autofocusing, channel alignment, ghost elimination, color correction, etc. ICM can capture the multispectral data with the spectral reflectance from 400nm to 700nm and wavelength interval of 20 nm. The 31 monochrome images with wavelength interval of 10 nm can reconstructed from 16 monochrome images under the 16 different wave-bands by using spectral reflectance reconstruction method. The reconstructed spectral reflectance curves are illustrate. The maximum size of the captured fabric sample is 100mm(width) $\times$ 80mm(height) and the corresponding image size is 1824 pixels (width) $\times$1344 pixels(height) which has 2,451,456 pixels.

The ICM system effectively overcomes the problem of the metamerism (i.e., two different colours having the same appearance under a specific light source) and offers a more rigorous and accurate means of colour management and quality control. This is a very important contribution in the textile industry. The specifications of the ICM system are shown in Table 2.1, the colour-difference data were obtained under D65 illumination for a 10° visual field.

Table 2.1 Specifications of the ICM system

Repeatability (NIST White Tiles)	Mean colorimetric error = 0.03 CMC (2:1)
Uniformity (NIST White Tiles)	Maximum and mean colorimetric errors = 0.1 and 0.01 CMC (2:1) units
Inter-instrument agreement between ICM system and benchmark spectrophotometer:	Maximum and mean spectral reflectance accuracy = 0.0089 and 0.0024 RMS errors Maximum and average colorimetric accuracy = 0.62 and 0.23 CMC (2:1) units
Measurement time	Less than 25 seconds
Spectral wavelength accuracy	±1 nm
Optical configuration	45° /10°
Spectral range	400 nm - 700 nm

Measurement sizes	100mm*80mm

2.4.2 Spectral Reflectance Reconstruction

Spectral reflectance reconstruction in multispectral imaging system (MIS) has attracted a lot of attention in recent years (Ville Heikkinen et al., 2007; Heikkinen et al., 2008; Y. Murakami, T. Obi, M. Yamaguchi, N. Ohyama, & Y. J. O. c. Komiya, 2001; Shen, Cai, Shao, & Xin, 2007; Shen, Xin, & Shao, 2007; N. J. I. T. o. I. P. Shimano, 2006; X. Zhang & Xu, 2008). The objective is to obtain a full spectral reflectance image of the objects (e.g., fabric) such that accurate colour reproduction can be performed. Applications of MIS also include fruit classification(Jiang & Gu, 2012), art archiving(J. Y. Hardeberg, Schmitt, & Brettel, 2002), and colour constancy determination(Mosny & Funt, 2006) among many others. In this study, multispectral imaging refers to using 16 narrow band channels to estimate the full spectral which consists of 31 channels, similarly as defined in reference (Shen, Cai, et al., 2007).

In MIS, spectral reflectance reconstruction refers to the process of reconstructing spectral reflectance from the response of multispectral image at different narrow-band wavelengths (Jon Y Hardeberg, 2001; J. Y. Hardeberg et al., 2002; Shen, Xin, et al., 2007). In most of the cases, there is a need to find a mathematical mapping to transform a camera's response vector (with dimension c) to a reflectance vector (with dimension m), where c is less than m.

2.5 Whiteness Measurement

Whiteness is an important property for many industries, such as textile and paper production(Aman, 2012; Coppel, Andersson, Neuman, & Edström, 2012; Gärtner & Griesser, 1975; Gay, Melo, & Hirschler, 2004; Imura, Imai, Kawabata, & Makino, 1997;

Jafari & Amirshahi, 2007; Puebla, 2006a; Uchida, 1998; Vik, Viková, & Periyasamy, 2015).

To make the whiteness different from the normal colour is the advent of florescent whitening agent (FWA)(Aman, 2012; Coppel et al., 2012). It absorbs energy from the short wavelength and emits them on the longer wavelength. That make the colour of the appearance not only depends on reflective part, but also on reflective part. It's very normal to find that many spectral factor even much larger than 100% over pure illuminant in 450nm wavelength.

2.5.1 Whiteness calculation

The calculation of whiteness should begin with the colour calculation. There are several whiteness formulas in textile measurement, the most recognized formula is CIE whiteness (Schanda, 2007). The formula is $W = Y + 800(x_n - x) + 1700(y_n - y)$ where Y is the Y-tristimulus value of the sample, x and y are the x, y chromaticity coordinates of the sample, and x_n, y_n are the chromaticity coordinates of the perfect diffuser, all for the CIE illuminant D65 and 1964 standard colorimetric observer. Limited to: $40 < W < 5Y - 280$.

2.5.2 Whiteness calibration

There are usually two methods for spectrophotometer to calibrate their UV light(Puebla, 2006b): one-point-matching and adjustable UV filter. One-point-matching method means UV filters will continuously move until the measurement reaches the target whiteness. The adjustable UV filter tries to combine two radiance factors (radiance with UV light and radiance with reduced UV light) to achieve a target value. This work extends these two methods in multispectral imaging system and compare the two results.

That will be detailly discussed in Chapter 4 Florescent whiteness measurement by multispectral imaging system.

2.6 Textile image analysis

In this section, some basic textile image analysis methods will be discussed.

2.6.1 Knitted fabric textile classification

Conventional yarn-dyed fabric classification often includes angle correction, directional projection, yarn segmentation and float point classification (C. F. J. Kuo, Shih, & Lee, 2004; Pan, Gao, Liu, Wang, & Europe, 2010; B. J. Xin, Hu, Baciu, & Yu, 2009; B. G. Xu, 1996; J. Zhang, Wang, Pan, Zhou, & Gao, 2018). It is not very easy for knitted fabric to identify by yarn segmentation and flat point classification since the yarns in knitted fabric are too soft and coupled together.

Although not many, there are two literature directly related to the work of knitted fabric classification. Tang-jun Lv and Hai-ru Long have applied the SURF algorithm to knitted fabric classification and recognition (Lv & Long, 2015). They first applied Gaussian denoise and then select the local feature. They make use of the reparability of patterns in the same fabric and use the SURF feature to match these patterns. Kuo and Kao have used the co-occurrence feature and SMO (self-organizing map) network to classify the knitted fabrics (C. F. J. Kuo & Kao, 2007). The disadvantage of co-occurrence feature is that it can only detect a small number of classes. For example, in Kuo and Kao's work, there are only 5 classes which are plain weave, twill weave, stain weave, single jersey, double jersey, and non-woven fabric.

2.6.2 Printing fabric analysis

Printed fabrics and other valuable textile materials have rich colours and variable patterns. Besides the fabric structural parameters (such as fabric densities, weave pattern), the colour pattern of printed fabrics is the most significant feature, which can be described by the number of colours, colour values, and patterns. Many researches have been done to measure fabric densities(Liu, Jiang, Liu, & Chai, 2014; Schneider, Gloy, & Merhof, 2014; J. Zhang, Xin, & Wu, 2014) and recognize weave pattern(Li, Wang, Deng, & Xin, 2020; Wang, Georganas, & Petriu, 2011). To the best of our knowledge, it is the first attempt to recognize colour pattern and measure fabric colours of printed fabrics by using multispectral image system.

The colour pattern recognition is indispensable for the textile and dying industries, including colour measurement and pattern segmentation, when reproducing the clients' standard samples or controlling the quality of the batch fabrics in production. Compared with manual colour pattern inspection, the automatic recognition method based on computer vision is more desirable to improve manufacturing efficiency and reduce the labour costs.

2.7 Summary

In this chapter, the literature about the multispectral imaging and textile images have been reviewed, with both perspectives from theory and applications. This thesis extends the theory and enrich the applications of using MSI in textile industry.

Chapter 3 Spectral reflectance reconstruction using L1-norm penalization for colour reproduction

3.1 Introduction

The literature of spectral reflectance has been reviewed. In this chapter, a new spectral reflectance reconstruction method will be proposed.

Spectral reflectance reconstruction in multispectral imaging (MSI) system has attracted a lot of attention in recent years (Ville Heikkinen et al., 2007; Heikkinen et al., 2008; Yuri Murakami et al., 2001; Shen, Cai, et al., 2007; Shen, Xin, et al., 2007; N. J. I. T. o. I. P. Shimano, 2006; X. Zhang & Xu, 2008). The objective is to obtain a full spectral reflectance image of the objects (e.g., fabric) such that accurate colour reproduction can be performed. Multispectral imaging has its advantage over the conventional three-channel colour imaging because it can provide the full spectral information in the visible band (i.e., 400nm - 700nm), which can be used for accurate colour measurement(Luo et al., 2015c)   . Applications of MSI also include fruit classification(Jiang & Gu, 2012), art archiving(J. Y. Hardeberg et al., 2002), and colour constancy determination(Mosny & Funt, 2006) among many others. In this study, multispectral imaging refers to using 16 narrow band channels to estimate the full spectral which consists of 31 channels, similarly as defined in (Shen, Cai, et al., 2007)

In MSI, spectral reflectance reconstruction refers to the process of reconstructing spectral reflectance from the response of multispectral image at different narrow-band wavelengths (Jon Y Hardeberg, 2001; J. Y. Hardeberg et al., 2002; Shen, Xin, et al., 2007). The transmission rate of a typical set of narrow band filters is shown in Figure

3.1. In most of the cases, there is a need to find a mathematical mapping to transform a camera's response vector (with dimension c) to a reflectance vector (with dimension m), where c is less than m.
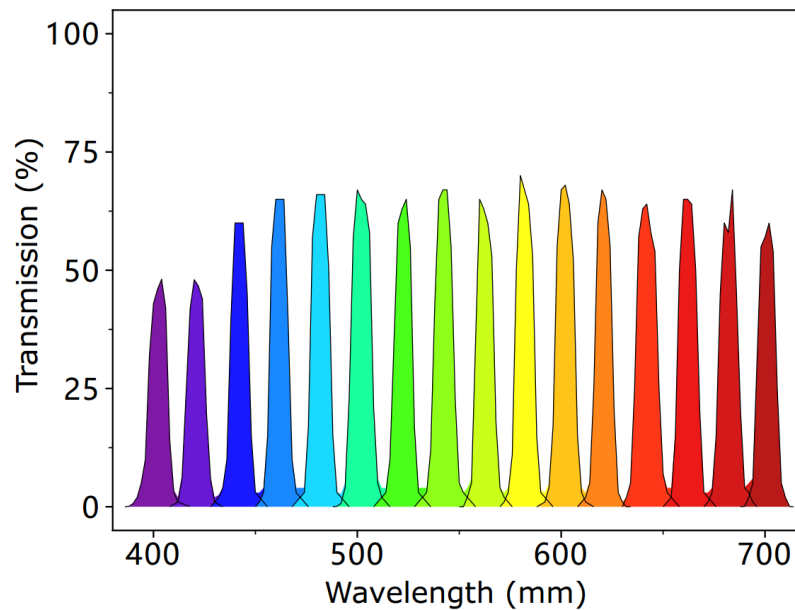

Figure 3.1 Transmission rate of 16 filters.

In the literature of multispectral imaging, several reflectance reconstruction techniques have been proposed, including Wiener estimation (Y. Murakami, T. Obi, M. Yamaguchi, N. Ohyama, & Y. Komiya, 2001; Shen, Xin, et al., 2007; N. J. I. T. o. I. P. Shimano, 2006), Least-square estimation method (Jon Y Hardeberg, 2001; J. Y. Hardeberg et al., 2002), and Kernel-based methods (V. Heikkinen et al., 2007; Heikkinen et al., 2008). These methods usually have too many parameters involved in estimating the mathematical mapping between the response and reflectance. Take Pseudo-Inverse as an example, it has mxc parameters, where m is the dimension of reflectance vector and c is the dimension of response vector. The number of parameters grow linearly with the value of c. In colour measurement applications(Herzog & Hill,

19

2003)it is not uncommon that the number of channels m and c are as large as 31 and 16 respectively, so the number of parameters will be 31 x 16=496. Because of large number of parameters, many training samples are needed for parameter estimation, otherwise such many parameters may cause overfitting in the reconstruction processing.

In this paper, a L1-norm penalization item is added to Least-square estimation to solve the overfitting issue. The L1-norm item can help the target parameter to achieve sparse property and overcome the overfitting problem in training. Here we take the Pseudo-Inverse as an example, if 5 out of the 16 channels contribute to the final reconstruction results of each reflectance, the number of parameters will decrease from 496 to 31 x 5=155, which decrease more than half of the parameters in the Pseudo-Inverse. In order to verify the results, we prepared 4 kinds of materials (cotton, paper, polyester, and nylon) with a total of 816 samples. The evaluation results verify the L1-norm penalization method can help to improve the colour reproduction accuracy compare to traditional methods.

The following part are organized as follows: Section 3.2 introduces the basic formulations in spectral reflectance reconstruction; Section 3.3 presents the current reconstruction algorithms; Section 3.4 discusses the proposed L1-norm method; Section 3.5 shows the experiments and the comparing results between our method and other methods; Section 3.6 and section 3.7 discuss the reason why the L1-norm works and reveal the conclusion of this work.

20

3.2 Formulation of multispectral imaging

In this work, a multispectral imaging system is built as illustrated in Figure 3.2. In the system, a monochrome camera is used for capturing the response images of each narrow-band wavelength λ_i $(1 < i < n)$ using the corresponding filter in the filter wheel. Narrow-band wavelength filters (transmission rate illustrated in Figure 3.1 and CCD cameras are commonly used in multispectral systems for colour measurement (Herzog & Hill, 2003; Luo et al., 2015a). The filter wheel with n filters is placed between the lens and the camera to filter the light entering the camera.
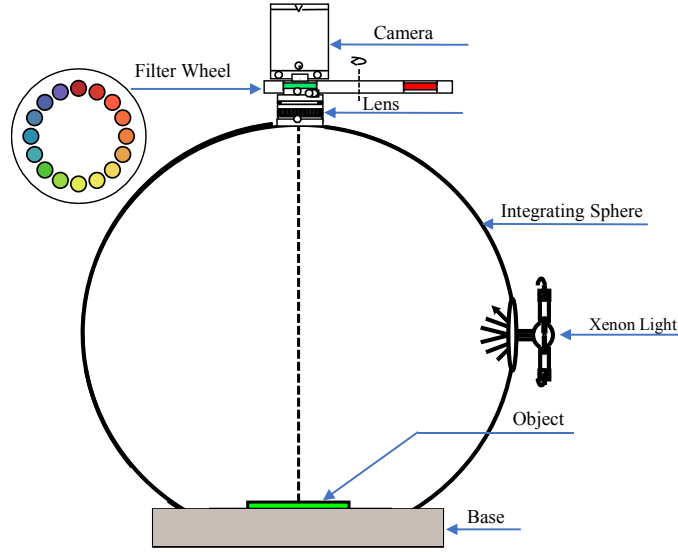

Figure 3.2 schematic diagram of proposed MSI.

The measured response of the camera is proportional to the intensity of light entering the sensor and we can formulate this as Equation (3.1). Denote $l(\lambda)$ to be the spectral power distribution of the imaging illumination, $r(\lambda)$ to be the spectral reflectance of

the samples being imaged, $s(\lambda)$ to be the sensitivity of CCD camera, b_c to be the bias response caused by dark current, and finally, n_c to be the noise. In spectral characterization of imaging system, spectral sensitivity and bias are recovered by training dataset with known reflectance.

Then these responses u_c of the c-th channel can be represented as

$$\begin{aligned} u_c &= \int l(\lambda)r(\lambda)s(\lambda)d\lambda + b_c + n_c \\ &= \int m_c(\lambda)r(\lambda)d\lambda + b_c + n_c \end{aligned} \tag{3.1}$$

The objective in reflectance reconstruction is to recover $r(\lambda)$. Note that $l(\lambda)$ and $l(\lambda)$ can be merged together into a single term $m_c(\lambda)$ in Equation (3.1).

In practice, the filters are narrow-band filters, so we can replace the continuous variables to their discrete counterparts and the integral can be replaced to summation. If N uniformly spaced samples are used over the visible spectrum, Equation (3.1) can be rewritten in vector and matrix notation as

$$\mathbf{u} = \mathbf{Mr} + \mathbf{b} + \mathbf{n} \tag{3.2}$$

where $\mathbf{u}$ is the c-dimensional vector and $\mathbf{b}$ is a \$m\$-dimensional vector, $\mathbf{M}$ is a c x m matrix of spectral responsivity and illumination, $\mathbf{b}$ and $\mathbf{n}$ are two vectors. $\mathbf{M}$ can be estimated by reference (Shen, Xin, et al., 2007).

3.3 Preliminaries

To make this work self-contained, this section briefly summarizes the formulations of typical reflectance reconstruction methods, including Least-square estimation, Ridge regression, Wiener estimation and Kernel methods. Our L1-norm based solution is built

based on Least-square estimation, and we will compare our method with Ridge regression and other methods.

3.3.1 Least-square estimation

The subsection provides a brief review of the Least-square estimation method, while reference (Jon Y Hardeberg, 2001)has a detailed discussion of the method. The estimation of reflectance is to find a c x m matrix $\mathbf{W}$ that can transform the response $\mathbf{u}$ into the estimated reflectance $\hat{\mathbf{r}}$,

$$\hat{\mathbf{r}} = \mathbf{W}\mathbf{u} \tag{3.3}$$

A natural thought will be to minimize the difference between the reconstructed $\hat{\mathbf{r}}$ and the Wu. So we can formulate the cost function as

$$E = \frac{1}{2} \| \mathbf{R} - \mathbf{W}\mathbf{U} \|_{\mathbf{F}}^{2} . \tag{3.4}$$

In this equation, $\mathbf{R}$ is the matrix form of $\mathbf{r}$ and $\mathbf{U}$ is the matrix form of $\mathbf{u}$. Note that the matrix $\mathbf{U}$ in Equation 3.4 is of size 16 x *number of samples*. The subscript F refers to the Frobenius norm. This equation has a closed-form solution and we can minimize it by derivative to $\mathbf{W}$.

In the Pseudo-Inverse technique, the transform matrix $\mathbf{W}$ is directly solved as

$$\mathbf{W} = \mathbf{R}\mathbf{U}^{\mathbf{T}}(\mathbf{U}\mathbf{U}^{\mathbf{T}})^{-1}, \tag{3.5}$$

where $\mathbf{R}$ denotes the matrix form of reflectance vector $\mathbf{r}$, and $\mathbf{U}$ denotes the matrix form of response vector $\mathbf{u}$.

3.3.2 Ridge Regression

Ridge regression can be viewed as adding an L2-norm penalization to Least-square estimation Equation 3.4, the cost function of ridge can be written down as

$$E = \frac{1}{2} \| \mathbf{R} - \mathbf{W}\mathbf{U} \|_{\mathbf{F}}^2 + \frac{1}{2}\boldsymbol{\beta}^2. \tag{3.6}$$

The closed form of solution $\mathbf{M}$ can be solved by partial differentiate $\mathbf{M}$ in both sides and make it equal to 0. The solution is

$$W = \mathbf{R}\mathbf{U}^{\mathbf{T}}(\mathbf{U}\mathbf{U}^{\mathbf{T}} + \boldsymbol{\beta}\mathbf{I})^{-1}. \tag{3.7}$$

3.3.3 Wiener estimation

In Wiener estimation (Shen, Cai, et al., 2007), the transform matrix is

$$\mathbf{W}_{\mathbf{WE}} = \mathbf{K}_{\mathbf{r}}\mathbf{M}^{\mathbf{T}}(\mathbf{M}\mathbf{K}_{\mathbf{r}}\mathbf{M}^{\mathbf{T}} + \mathbf{K}_{\mathbf{n}})^{-1}, \tag{3.8}$$

where $\mathbf{K}_{\mathbf{r}}$ and $\mathbf{K}_{\mathbf{n}}$ are the autocorrelation matrices of reflectance and noise, respectively:

$$\mathbf{K}_{\mathbf{r}} = \mathbb{E}(\mathbf{r}\mathbf{r}^{\mathbf{T}}), \tag{3.9}$$

$$\mathbf{K}_{\mathbf{n}} = \mathrm{diag}\{\boldsymbol{\sigma}_{\mathbf{1}}^{\mathbf{2}}, \boldsymbol{\sigma}_{\mathbf{2}}^{\mathbf{2}}, \cdots, \boldsymbol{\sigma}_{\mathbf{c}}^{\mathbf{2}}\}. \tag{3.10}$$

The noise is assumed to be independent across each channel, so the matrix k_n is a diagonal matrix in Wiener estimation. The noise σ_c can be estimated as:

$$\hat{\sigma}_c^2 = \mathbb{E}\left(\| \mathbf{u}_{\mathbf{c}} - \mathbf{m}_{\mathbf{c}}\mathbf{r} \|_{\mathbf{F}}^2\right), \tag{3.11}$$

where $\mathbf{u}_{\mathbf{c}}$ is the response of the c-th channel, and $\mathbf{m}_{\mathbf{c}}$ is the spectral responsivity of the c-th channel. $\mathbb{E}$ denotes the operation of expectation.

3.3.4 Kernel method

Kernel method is also widely used in spectral reflectance reconstruction(V. Heikkinen et al., 2007; Heikkinen et al., 2008). It regularizes Least-square regression in Reproducing Kernel Hibert Space (RKHS). Kernel can be viewed as a function to map the vector in Least-square method to a new space. There are many kernels which can be used, in the work (Heikkinen et al., 2008), the authors applied Gaussian kernel, Polynomial kernel, Spline kernel and Duchon kernel.For example, Guassian kernel can be defined by

$$k(\mathbf{x}, \mathbf{z}) = \exp\left(-\frac{\|\mathbf{x} - \mathbf{z}\|}{2\sigma^2}\right),$$ (3.12)

where $\sigma > 0$ is a super-parameter. The Gaussian kernel is invariant to rotation and translation, so $k(\mathbf{x}, \mathbf{z}) = k(\|\mathbf{x} - \mathbf{z}\|)$. The corresponding RHKS space is infinite dimensional.

3.4 Proposed method

In this work, we propose to apply the L1-norm penalized linear regression method for reflectance reconstruction. To the best of our knowledge, it is the first study to use the L1-norm penalized linear regression method for this kind of application. The L1-norm can provide the constrained variable (in this work the constrained variable is $\mathbf{W}$) with sparsity, and this can help to overcome overfitting (Boyd, Parikh, & Chu, 2011). The cost function of L1-norm penalized linear regression in reflectance reconstruction is

$$E = \frac{1}{2} \|\mathbf{R} - \mathbf{WU}\|_{\mathbf{F}}^2 + \boldsymbol{\alpha} \|\mathbf{W}\|_{\mathbf{1}}.$$ (3.13)

In this equation, α is a super-parameter (or a regularization parameter) and can be estimated by cross validation. Because the L1-norm is not smooth, we can use Alternation Direction Method of Multipliers(ADMM)(Boyd et al., 2011) to solve it. A dummy variable can be introduced to Equation 3.13, and it will be transformed as:

$$\mathbf{W}, \mathbf{Z} = \arg \min_{\mathbf{W}, \mathbf{Z}} \frac{1}{2} \| \mathbf{R} - \mathbf{W}\mathbf{U} \|_{\mathbf{F}}^2 + \boldsymbol{\alpha} \| \mathbf{Z} \|_{\mathbf{1}} \tag{3.14}$$
$$s.t \qquad \mathbf{W} = \mathbf{Z}.$$

This is a standard lasso (least absolute shrinkage and selection operator) problem and we can solve it by the following iteration(Boyd et al., 2011).

$$\mathbf{W}^{\mathbf{k+1}} = (\mathbf{R}\mathbf{U}^{\mathbf{T}} + \boldsymbol{\mu}\mathbf{Z}^{\mathbf{k}} - \mathbf{T}^{\mathbf{k}})(\mathbf{U}\mathbf{U}^{\mathbf{T}} + \boldsymbol{\mu}\mathbf{I})^{-1} \tag{3.15}$$

$$\mathbf{Z}^{\mathbf{k+1}} = \mathrm{soft}(\mathbf{W}^{\mathbf{k+1}} + \frac{\mathbf{T}^{\mathbf{k}}}{\mu}, \frac{\alpha}{\mu}\mathbf{I}) \tag{3.16}$$

$$\mathbf{T}^{\mathbf{k+1}} = \mathbf{T}^{\mathbf{k}} + \boldsymbol{\mu}(\mathbf{Z}^{\mathbf{k+1}} - \mathbf{W}^{\mathbf{k+1}}) \tag{3.17}$$

where matrices $\mathbf{Z}$, $\mathbf{T}$ are intermediate variables, which can be initialized with zero matrices and μ should be set larger than zero and $\mathbf{I}$ is a unit matrix.

The operation soft is a soft-thresholding function as:

$$\mathrm{soft}(u, c) = \mathrm{sign}(u) \max\{|u| - c, 0\} \tag{3.18}$$

Equation 3.13 can be efficiently solved by using the toolbox in (Boyd et al., 2011).

3.5 Experiments and results

3.5.1 Data preparation

Four kinds of materials are prepared for testing and they are polyester, nylon, paper and cotton. We use one kind of sample (e.g., polyester) as the training set and all the 4 kinds

of materials as testing set (i.e., polyester, nylon, paper and cotton). The objective is to test whether the accuracy of spectral reflectance reconstruction is depending on the type of the materials used for training / testing. Each texture includes 204 patches and the reflectance of the colour patches were measured using a Spectrophotometer DataColor D650 with an interval of 10nm. The reason for using the Spectrophotometer is because it is the standard for colour measurement(Schanda, 2007). The multispectral images of these samples are acquired by a self-made machine as shown in Figure 3.2. We use a Xeon lamp and the integral sphere as the illumination light source to make the light more uniform. Besides, a high-resolution monochromatic camera is employed to capture the multispectral images.

The L*a*b space scatters of each texture are shown in Figure 3.4. The values of this samples are computed by computational colour sicence tools(Westland et al., 2012). The reflectance of the samples are in the range of 400nm-700nm sampled with 10nm intervals. The x-axis indicates the wavelength and the y-axis indicates the reflectance measured by the Spectrophotometer.

3.5.2 Evaluation metric

The colour accuracy of the reflectance reconstruction is evaluated both in spectral and colourimetric error. The spectral Root-Mean-Square RMS error between the actual reflectance $\mathbf{r}$ and its estimate $\hat{\mathbf{r}}$ is calculated as

$$RMS = \left(\frac{(\mathbf{r}-\hat{\mathbf{r}})^T (\mathbf{r}-\hat{\mathbf{r}})}{m} \right)^{1/2} \tag{3.19}$$

where *m* is the dimension of vector **r**. The colour difference is evaluated by ΔE (Schanda, 2007), which is widely used in many industries such as textile and paper production.

3.5.3 Super-parameter estimation

There are 3 super-parameters in our experiments that need estimation, the β in Equation 3.6, the α in proposed method in Equation 3.13 and the γ in Equation 3.19. These parameters are estimated by cotton samples only, 70% percent of 204 cotton samples are used for training and the remaining 30% are used for validation. The results are plotted in Figure 3.3. The γ, α and β are set to 0.006, 0.074 and 0.0005 respectively.
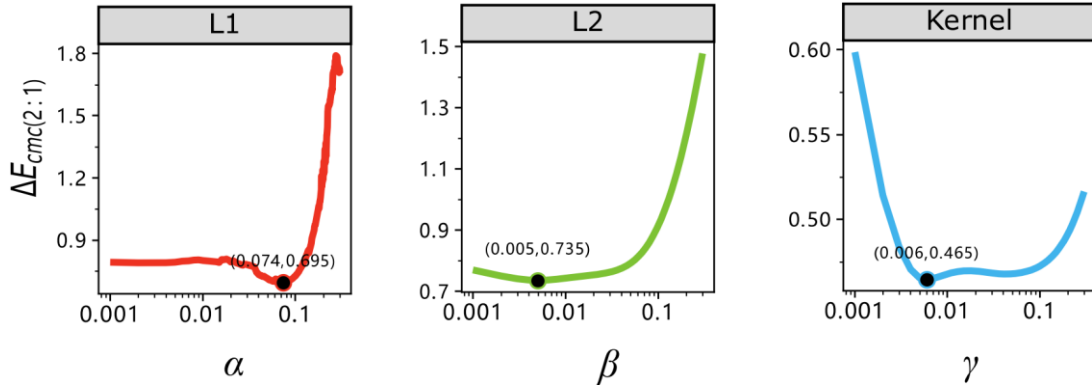
Figure 3.3 Super-parameter estimation of α, β and γ in our experiment, the y-axis is the colourimetric difference between the reconstructed spectral and ground truth spectral reflectance. The black point is the minimum point of the ΔE, which means the value we will adopt in the reconstruction.

(a) L*a*b scatter of cotton samples

(b) L*a*b scatter of polyester samples

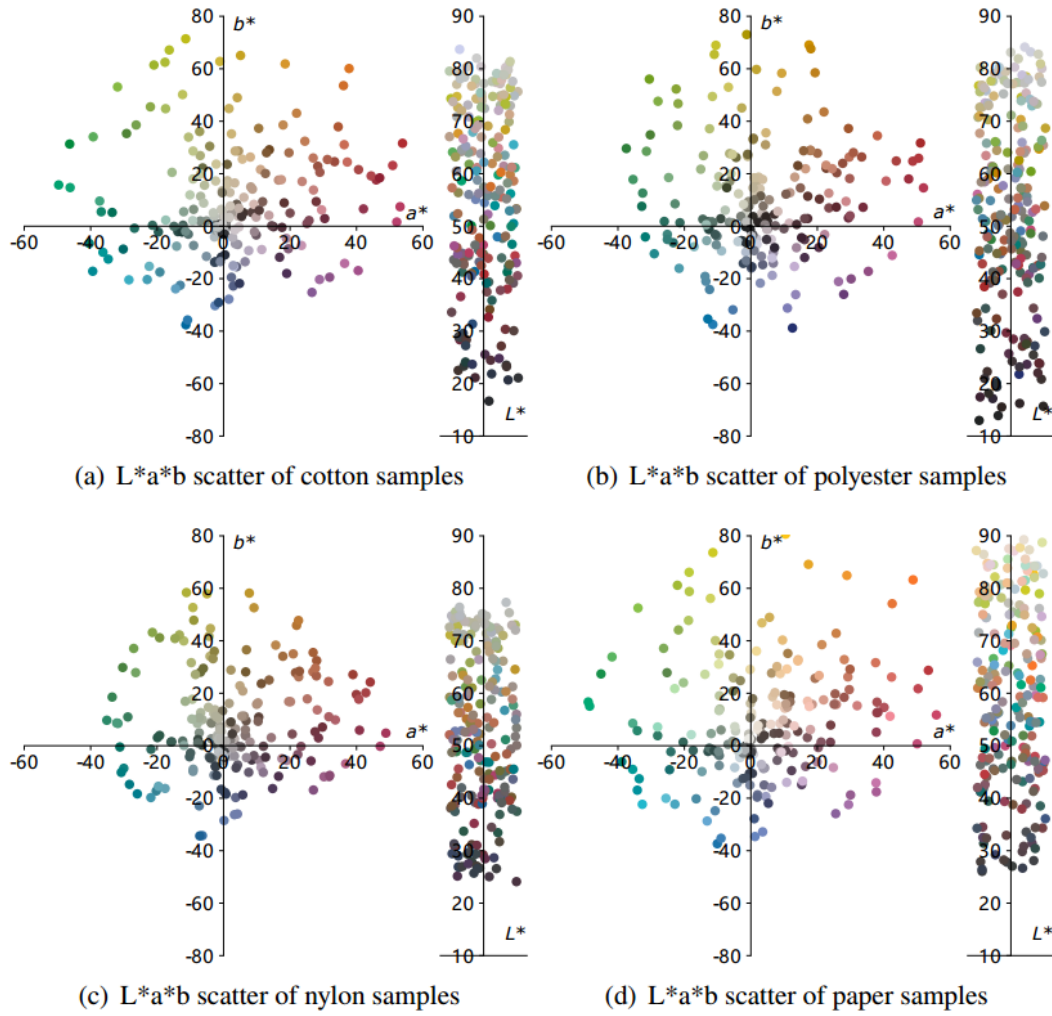(c) L*a*b scatter of nylon samples

(d) L*a*b scatter of paper samples

Figure 3.4 The L*a*b scatter of cotton, polyester, nylon and paper. The reflectance are measured by DataColor D650 with 10nm interval, gloss include and 9mm spot size. L*a*b values are computed by computational colour tools(Westland et al., 2012).
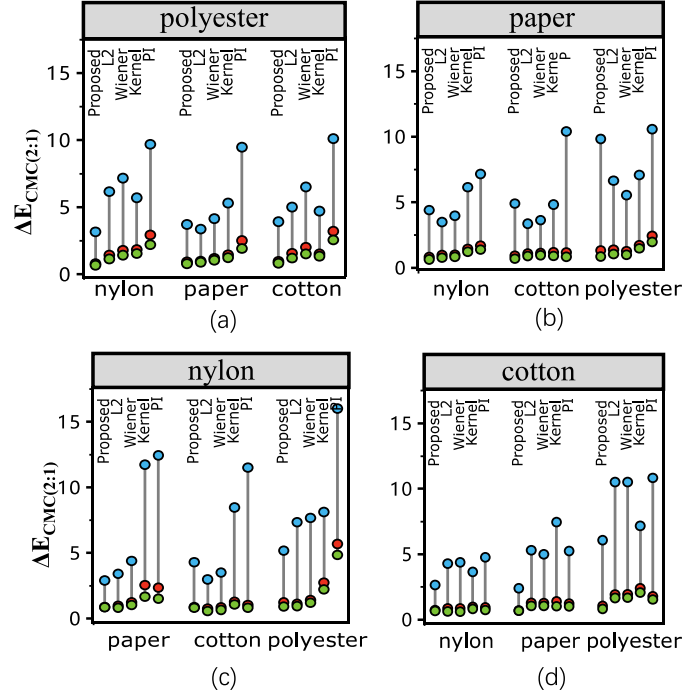
3.5.4 Results

Figure 3.5 ΔE results under illumination D65. (a) is polyester as training; (b) is paper as training; (c) is nylon as training and (d) is the cotton as training.

Figure 3.5 illustrates the results when one kind of textures (e.g., cotton) is used as training set (204 samples) and others (204 x 3 samples) as testing set. The colour difference values under D65 are shown in the figure. In figure 3.5, the L1-norm method outperforms the Pseudo-Inverse and other estimation methods in all cases when the training set is different from the testing set. The results are consistent when using the mean, the median and the maximum of the colour differences after reflectance reconstruction for the comparison. The mean and median results reveal the overall performance, while the worst case performance is shown in the maximum colour difference results. Specifically, the results of L1-norm consistently outperform that of the Pseudo-Inverse method using the mean colour difference when the training material is different from the testing material. When using the median for the comparison, L1-norm is better than the pseudo-inverse method in the nylon material for all the testing

sets. Similar results are also obtained when using the maximum colour difference for comparison in the nylon material. Overall, in the situation when the testing material is unseen (i.e., not present in the testing set) which is often in practice, using L1-norm is better than using Pseudo-Inverse and Wiener estimation for spectral reflectance reconstruction.
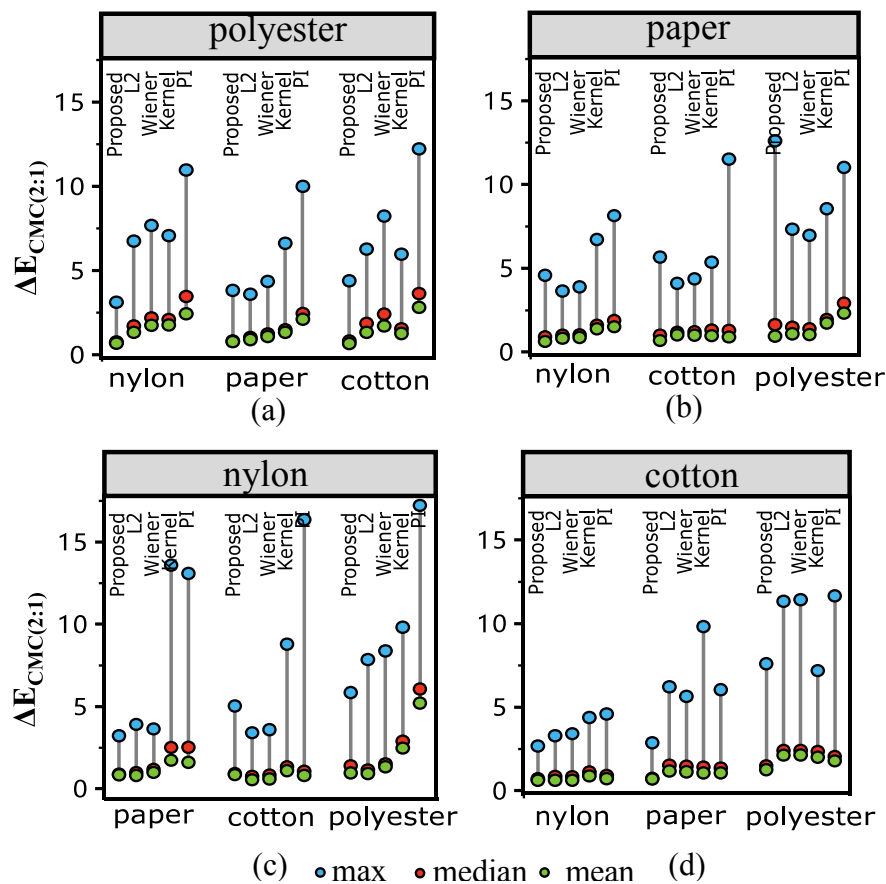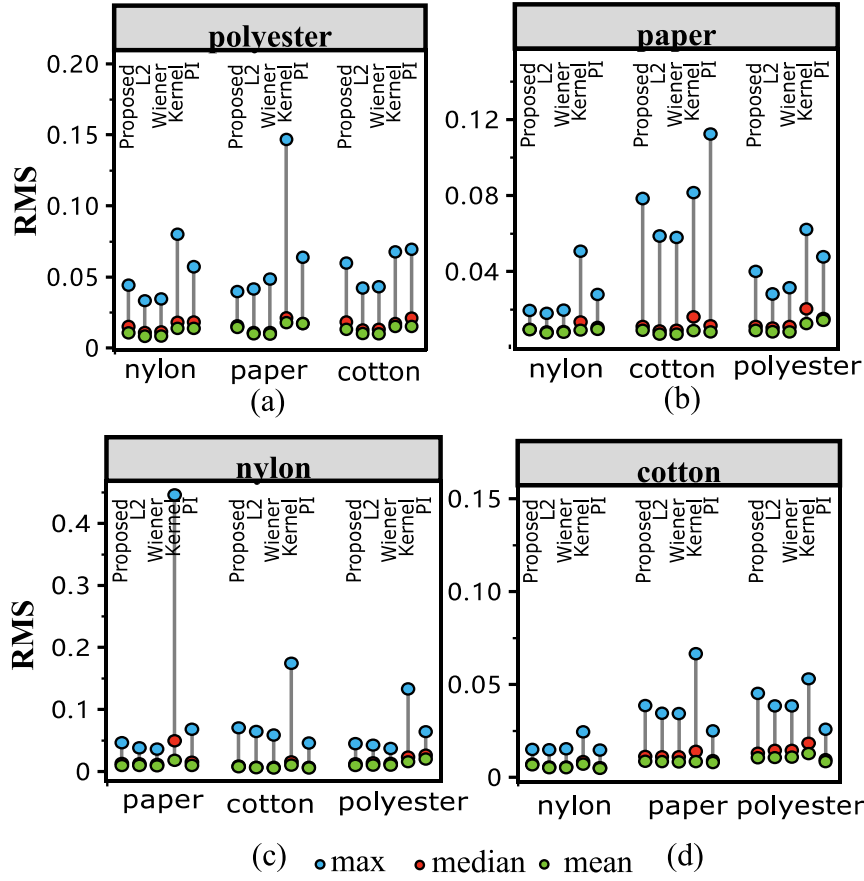

Figure 3.6 ΔE results under illumination F2. (a) is polyester as training; (b) is paper as training; (c) is nylon as training and (d) is the cotton as training.

Figure 3.7 RMS results of spectral reflectance reconstruction. (a) is polyester as training; (b) is paper as training; (c) is nylon as training and (d) is the cotton as training.

Figure 3.6 shows the values of the colour difference with illumination F2. The results tend to be similar to that of Figure 3.5. Figure 3.7 shows the spectral difference between the reflectance measured by Spectrophotometer and MSI using RMS which is not in the colour space. From the results, it is interesting to note that the L1-norm method does not show significant advantage over Pseudo-Inverse and Wiener estimation when using RMS to measure the difference. In practice, colour difference is measured in the colour space (D65 and F2 in Figure 3.5 and Figure 3.6 respectively). This reveals that L1-norm can be used in practical situations.
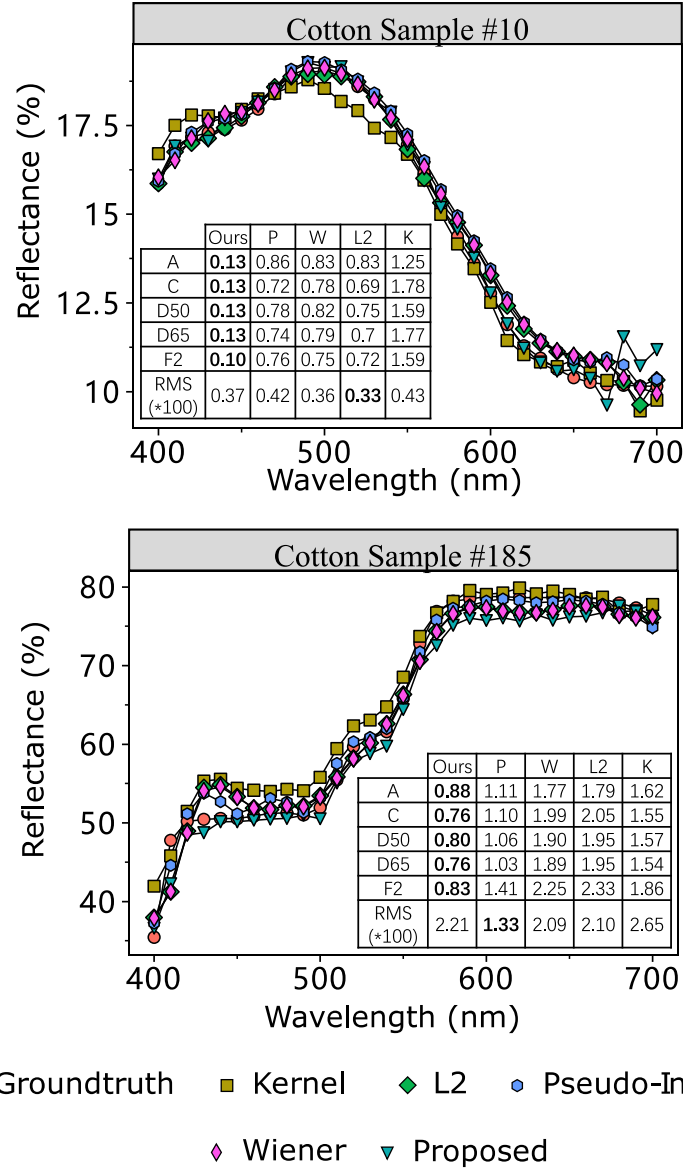
Cotton Sample #10

	Ours	P	W	L2	K
A	**0.13**	0.86	0.83	0.83	1.25
C	**0.13**	0.72	0.78	0.69	1.78
D50	**0.13**	0.78	0.82	0.75	1.59
D65	**0.13**	0.74	0.79	0.7	1.77
F2	**0.10**	0.76	0.75	0.72	1.59
RMS (*100)	0.37	0.42	0.36	**0.33**	0.43

Cotton Sample #185

	Ours	P	W	L2	K
A	**0.88**	1.11	1.77	1.79	1.62
C	**0.76**	1.10	1.99	2.05	1.55
D50	**0.80**	1.06	1.90	1.95	1.57
D65	**0.76**	1.03	1.89	1.95	1.54
F2	**0.83**	1.41	2.25	2.33	1.86
RMS (*100)	2.21	**1.33**	2.09	2.10	2.65

Legend: ● Groundtruth   ■ Kernel   ◆ L2   ● Pseudo-Invese   ◆ Wiener   ▽ Proposed

Figure 3.8 Reflectance reconstruction of a paper sample of the proposed L1-norm estimation and traditional estimations when using cotton for training. Tables inside the plots are the colour difference and spectral difference. The A, C, D50, D65 and F2 represents different illumination. The unit of these item is $\Delta E(cmc(2:1))$. RMS represents the Root-Mean-Square spectral difference metric. In the tables, method "P" is the briefcase of method Pseudo-Inverse. "Ours" is the proposed method. "W" is Wiener estimation. "K" means kernel method.

3.6 Discussion

This section discusses the reason for the superior results using L1 penalization.

As is mentioned in the section 3.4, L1 penalization can overcome the overfitting. Each materials has its special property on the reflectance(Shiradkar, Shen, Landon, Heng Ong, & Tan, 2014), which also can be confirmed by Figure 3.6. Figure 3.6 plots the first 4 feature vectors of the 4 materials, where we can find the samples have a great difference especially for the paper samples. When using the traditional methods with no penalty to reconstruct the spectral reflectance, the internal-texture property is easily to learn. What we can do is to prevent the learning system from learning an internal property. That's why when using the unseen texture samples as testing, the error is larger than the same texture as training.
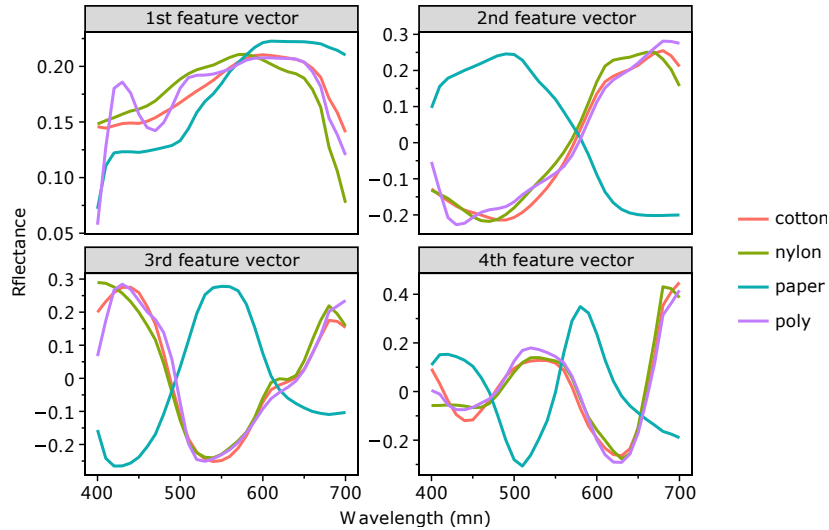
Figure 3.9 The first 4 feature vectors of 4 kinds samples (cotton, polyester, nylon and paper).

A penalization item can be viewed as an prior knowledge to the object function(Bishop, 2006). As we using the narrow-band filters in our system, an easy constrain can be found, which is the target value can on decided by its neighbour channels. All the 16 filters are shown in the Figure 3.1. Take the 500nm center filter as an example, the filter blocks most of the light in the spectral domain but keeping some of the light from 490nm to 520nm to pass through. So if we reconstruct the reflectance in 595nm to

605nm in our target results, it should have little to no relationship with the response from 490nm to 520nm. By adopting the L1 penalization, the weight of this unrelated channel can be reduced to 0.

This sparsity characteristic can also be verified in Figure 3.10, the reflectance curves measured by the Spectrophotometer and the response curve captured by MSI share a similar shape. It can also be confirmed that the reflectance curve should only be constructed by its neighborhood channels during reflectance reconstruction.
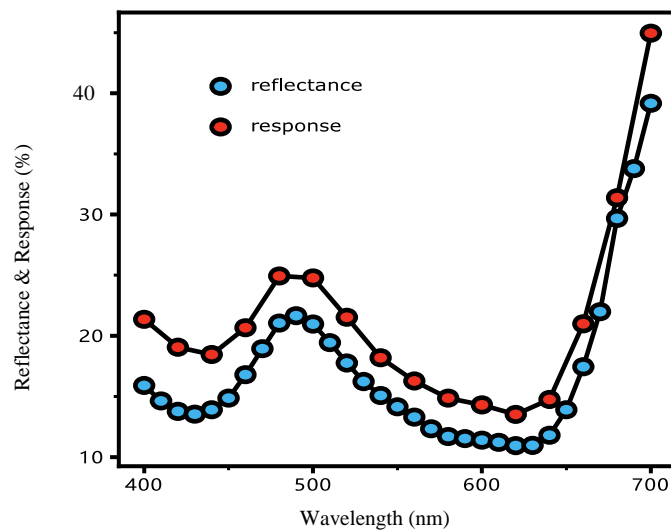
Figure 3.10 The reflectance and response of a typical cotton sample. The response is 16-d vector measured by a self-made MSI and reflectance is a 31-d vector measured by a Spectrophotometer.

Based on sparsity characteristic of reflectance, the superior performance of the L1 penalization method is reasonable and understandable. It can inhibit the noise introduced by the similar textures and only focus on the accuracy introduced by the MSI.

3.7 Conclusion

We propose a L1-norm method for reflectance reconstruction which in certain practical conditions (when the testing texture is unavailable in training samples), the accuracy of the reconstructed reflectance is higher than that using the conventional methods like Pseudo-Inverse and Wiener estimation method. Note that this study is mainly focus on colour reproduction, therefore other metrics such as shape-distance sensitivity are not included.

In this paper, we also find a very interesting phenomenon that while we are optimizing the colour difference by spectral domain, the results of proposed method are better in the colour domain. This does not affect practical application of the proposed method because colour difference is measured mainly in colour domain. This phenomenon can be investigated in future work.

Chapter 4 Florescent whiteness measurement by multispectral imaging system

4.1 Introduction

In the previous chapter, the reflectance reconstruction has been studied. Accurate colour information can be obtained by various equations depending on light source and viewing conditions with spectral reflectance (Westland et al., 2012). Compared to spectrophotometer, there is still a disadvantage of the MSI for colour measurement which is that it cannot measure whiteness with the device presented in previous chapters.

Whiteness measurement has been an important aspect for industries like textile, paper and detergent production. A large batch of fabric samples with inconsistent whiteness would be rejected by a client which could incur financial impacts on the fabric manufacturer. Traditional whiteness measurement is based on spectrophotometers, such as DataColor 650 and X-Rite Ci7860, which are very effective in measuring whiteness and they are used as the standard instrument in the industry. However, the limitation in using spectrophotometers is that one can only measure the average reflectance of an area without any spatial information. On the other hand, MSI has the advantage over spectrophotometer due to its ability to capture spatial information. However, there are very little study in the literature on the whiteness measurement capability of MSI in the presence of fluorescent whitening agents (FWAs). This study provides strong evidence that MSI can be used for accurate whiteness measurement as well as ensuring spatial uniformity.

The major contributions are:

(1) A practical and novel multispectral imaging machine for whiteness measurement is built by which the accuracy of whiteness measurement is as high as industry standard;

(2) An adjustable UV illumination box is designed by which the ratio of UV to visible light can be adjusted. The method shows high stability and robustness in colour and whiteness measurement, which will greatly contribute to the colour measurement and quality control in textile and paper production industry;

(3) A theoretical model is developed and applied to the colour measuring process in the multispectral imaging machine which can ensure the spatial uniformity for both materials with and without FWAs added.

4.2 Formulation of MSI whiteness measurement

We will introduce how to calculate the whiteness metric by equations. Besides, by the mathematical depicts, the spatial uniformity should be satisfied.
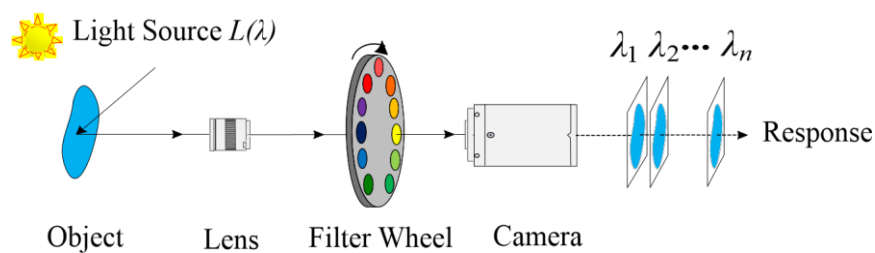
Figure 4.1 Schematic diagram of filter wheel multispectral imaging system

When we want to collect the resp data, we should first sequentially turn the filter wheel and in each channel, a raw grey image is acquired. This un-processed image is called raw Response in our project as shown in Figure.

After we collect the raw response data, the second procedure is pre-processing the data, and transform these image data to whiteness metric. We balance the raw response data by Equation 4.1.

$$p_o(i, j) = \frac{Resp(i, j)}{White(i, j)} \tag{4.1}$$

Figure 4.2 Dataflow of this processing.

4.2.1 Spatial uniformity proof

Colour measurement of whiteness should follow the spatial uniformity, that means the same material in different coordinate of the object should be the same. That's a challenge to multispectral imaging, in this subsection, we will prove our measurement is spatial uniform.

$$p_o(\lambda) = p_r(\lambda) + p_f(\lambda) \tag{4.2}$$

Where $p_o(\lambda)$ is the radiance factor of material, $p_r(\lambda)$ and $p_f(\lambda)$ are pure reflectance and florescence part respectively. By definition, $p_f(\lambda)$ can be written as

$$p_f(\lambda) = \left(\sum_{\lambda'} l(\lambda')\alpha(\lambda') \right) e(\lambda) \tag{4.3}$$

where $l(\lambda')$ is the illumination in the wavelength λ from the light source, $\alpha(\lambda')$ is the absorption ratio of the fluorescence material in wavelength λ' and $e(\lambda)$ is the emit ratio of the fluorescence material in wavelength λ. The fluorescence material absorbs light in wavelength bands λ' which are usually in the UV region and emits light in a particular wavelength band λ (e.g., 450nm).

As FWAs absorbing a narrow wavelength band in UV, it can be assumed that $l(\lambda)'$ and $a(\lambda')$ are constant across the wavelength bands λ' (Y. Fu, Lam, Kobashi, et al., 2014; Y. Fu, Lam, Matsushita, et al., 2014; Y. Fu et al., 2013; Y. Fu et al., 2018). In this project, we denote the light without passing from the filter GG395 as UV100, because it includes 100% UV light; we denote the light passing through GG395 as UV0.

For simplicity, denote p_f in UV0 as p_{f0}, p_f in UV100 as p_{f100} and p_f in our desired light as p_{fd}. Under our assumption,

$$p_{f0}(\lambda) = l_0 \times a \times e(\lambda) \tag{4.4}$$

and

$$p_{f100}(\lambda) = l_{100} \times a \times e(\lambda) \tag{4.5}$$

Similar to reference(Yang, 2017), we can formulate the intensity under our desired light source(such as D65 or D50) as

$$p_{od} = \alpha p_{o0} + (1-\alpha) p_{o100} \tag{4.6}$$

The linear combination method enables the relighting of white sample by changing the parameters. The one-point-matching method just provide a radiance factor of spectrum image, but from the linear combination method we can get the UV ratio of our Xenon lamp and relight the sample with a new light.

4.2.2 Spatial uniformity for pure reflective material

As reference (Y. Fu, Lam, Matsushita, et al., 2014), we formulate the observed spectrum of an ordinary reflection at wavelength λ can be expressed as

$$pr(\lambda, x, y) = l(\lambda, x, y) \times s(\lambda, x, y) \tag{4.7}$$

where $l(\lambda, x, y)$ is the spectrum of the incident light at wavelength λ at coordinate (x, y). So, the spectrum is linear to the light intensity and $s(\lambda, x, y)$ is the spectral reflectance of the material at wavelength λ.

where $pw(\lambda, x, y)$ is the observed spectrum of balance board and the $sw(\lambda, x, y)$ is equal at any coordinates (x, y). So, for any coordinates (x_1, y_1) and (x_2, y_2). if $s(\lambda, x_1, y_1) = s(\lambda, x_2, y_2)$, then $resp(\lambda, x_1, y_1) = resp(\lambda, x_2, y_2)$. That means our system are spatial uniform everywhere for pure reflective material surface.

4.2.3 Spatial uniformity for materials with FWAs

Substitute Equation (4.7) and (4.3) to (4.2), it evident the spatial uniformity for material with FWAs.

Combined the upper equation, we can find the

$$
\begin{aligned}
p_o(\lambda, x, y) &= p_r(\lambda, x, y) + p_f(\lambda, x, y) \\
&= l(\lambda, x, y)s(\lambda, x, y) + l_{uv}(x, y)a_{uv}(x, y)e(\lambda) \\
&= l(\lambda, x, y)s(\lambda, x, y) + k \times l(\lambda, x, y)a_{uv}(x, y)e(\lambda) \\
&\propto l(\lambda, x, y)
\end{aligned}
\tag{4.8}
$$

As only one light used in UV0 and UV100 exclusively, the ratio of UV light to visible light should be constant, i.e. $k \times l(\lambda, x, y) = luv(x, y)$. So, the $p_o(\lambda, x, y)$ will be linear to $l(\lambda, x, y)$. That means, by light balance, the spatial uniformity is ensured. In the light of UV0, k should be close to 0.

4.2.4 Whiteness formula

There are several whiteness formulas now, according to AATCC 110 in textile industry, the well acceptable whiteness formula is CIE whiteness formula. (Schanda, 2007) The formula is

$$W = Y + 800(x_n - x) + 1700(y_n - y)$$

$$\text{Limited to: } 40 < W < 5Y - 280 .$$

(4.9)

where Y is the Y-tristimulus value of the sample, x and y are the x, y chromaticity coordinates of the sample, and x_n, y_n are the chromaticity coordinates of the perfect diffuser, all for the CIE illuminant D65 and 1964 standard colourimetric observer.

4.3 Experimental details

This section describes the device used in experimentation, the dataset involved, the results and corresponding discussion for whiteness measurement and spatial uniformity testing.

4.3.1 Device setup

A new multispectral imaging system (J. H. Xin, Shen, & Ge, 2020a, 2020b) is built for this work. The sketch of the system is shown in Figure 4.3. Unlike conventional multispectral imaging systems which often use Tungsten lamp as the illumination source, we use a novel integrating sphere illumination system. Moreover, an UV adjustment box (shown in Figure 4.3), mounted with two filters, one for blocking UV light (GG395, Yellow filter in Figure 4.3) and another for blocking visual light (UG1, Violet filter in Figure 4.3) is placed between the Xenon lam and the integrating sphere to control the amount of UV light and visible light passing into the sphere.

Using the new illumination system, we can have a better control to the ratio of UV light to visible light in the light-source to illuminate the object which results in a more versatile light-source. Besides, the integrating sphere helps to diffuse the light and improves the spatial uniformity of the light-source.
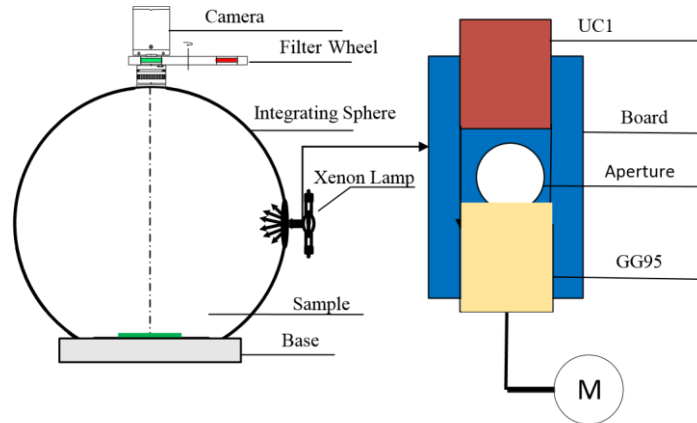
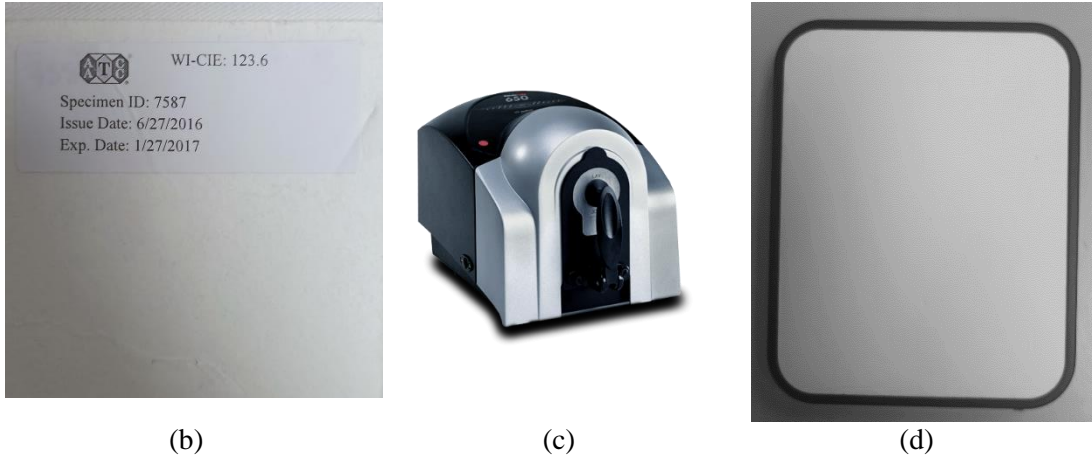Figure 4.3 Sketch of building machine

(a)

(b)	(c)	(d)
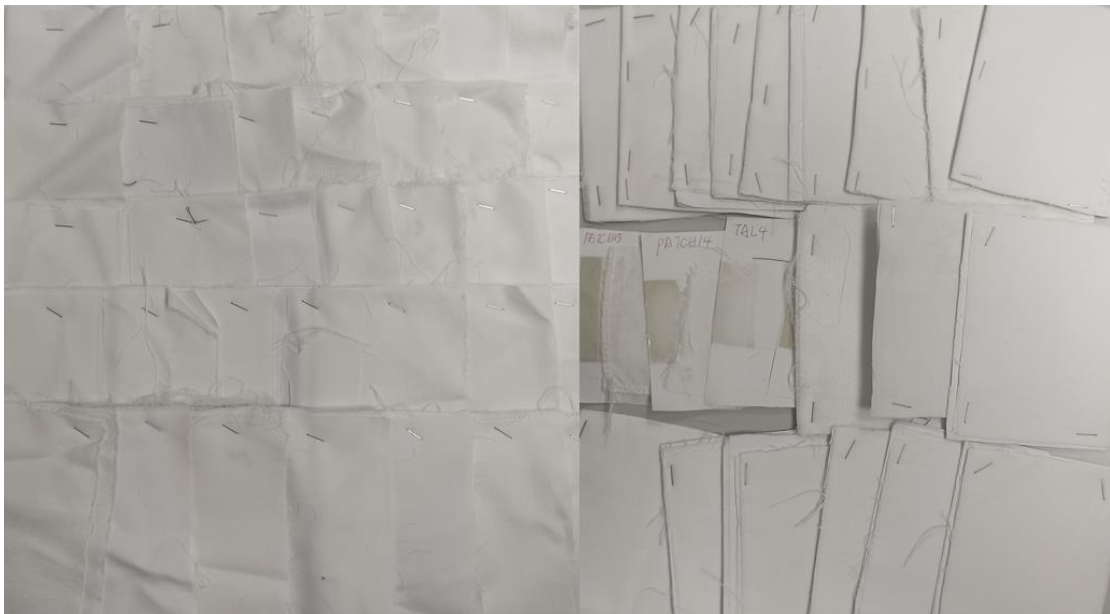
Figure 4.4 Device and samples used in experiment. (a) 64 testing samples with FWAs; (b) Calibration samples from AATCC; (c) DataColor 650 for comparison and Ground truth; (d) BaSO$_2$ white board for spatial calibration and white calibration.

4.3.2 Dataset

To investigate the performance of whiteness measurement, 64 white samples which cover the full white space in the visible spectrum are used. 10 of them are from factories, the others are dyed with different FWAs and cotton fabrics.

The spectral and whiteness values of these samples are measured by spectrophotometer (DataColor 650) as the ground truth.

Besides, a standard AATCC fluorescence whiteness sample is prepared, and it is used to calibrate the MSI for the one-point-matching method(AATCC, 2018).

4.3.3 Whiteness Calibration

There are two classical calibration methods in Spectrophotometer for whiteness calibration. They are one-point-matching method and numerical method. Both calibration operations are conducted in our system.

44

4.3.4 One-point method and numerical method

One-point-matching measurement method and numerical UV adaption method are compared in our experiment. For the one-point-matching method, we continuously adjust the position of the UV filter (each step of 2mm) to measure the difference between the measured whiteness value and the standard whiteness value (from AATCC). The position of the UV filter with the smallest difference is recorded. Then we treat this UV filter position as our standard UV position. The procedure of the one-point-matching method is shown in Figure 4.4. For the numerical UV adaption method, we set the fabric in two different position UV0 and UV100, and then combine the two images into one.
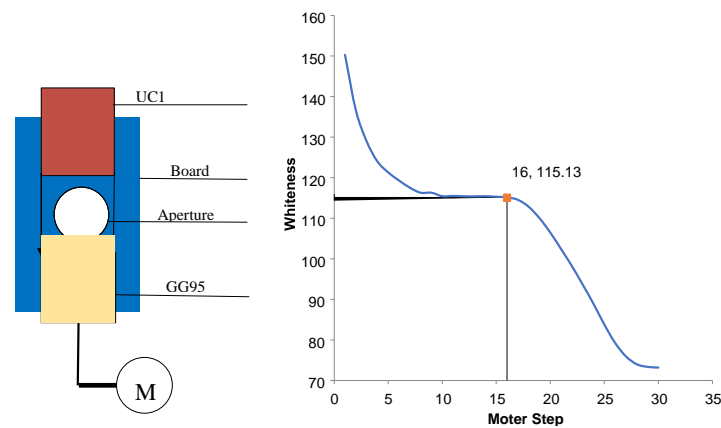
Figure 4.5 One-Point-Matching Whiteness Calibration Method. The x axis is the motor steps and when it slowly moves, the whiteness of the fabric (y axis) decrease slowly. When the motor move to the red point, it will stop and set the UV position as the standard position.

The results of unicameral UV adjustment and One-Point-Matching calibration method comparison is illustrated in Figure 4.5.
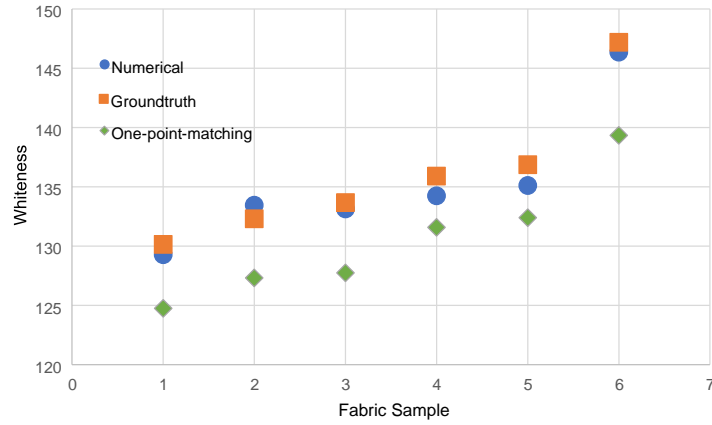
Figure 4.6 Results of unicameral UV adjustment and One-Point-Matching calibration method comparison.

The green diamond point is one-point-matching calibration method results. It is continuous less than the ground truth from calibrated spectrophotometer while the Numerical method is much closer to the ground truth. An easy explain of this is that: the calibration of the one-point-matching method is much longer in calibration step than measuring step.

It will heat the calibration samples in the calibration step, and it takes less time when practical measuring a sample. By one-point-measuring calibration method, the calibration time consuming is the same as testing step. It will be much accurate for numerical method.

4.3.5 Spatial Uniformity

In our experiment, we cut a pure white fabric with FWAs and the same material everywhere and evenly cut it into 12 parts, as shown in the picture, with 3 rows and 4 columns. Then calculate the average spectral reflectance for each pixel of the fabric of each part, and calculate the whiteness according to the spectral reflectance. We will find that the spectral reflectance is almost the same, and the value of whiteness is also

very different. This proves that our system is indeed spatial uniform. As shown in Figure 4.6.

W=146.87 **W=148.96** **W=148.81** **W=149.94**

W=146.94 **W=147.45** **W=147.30** **W=149.34**

W=145.94 **W=146.91** **W=147.13** **W=148.23**
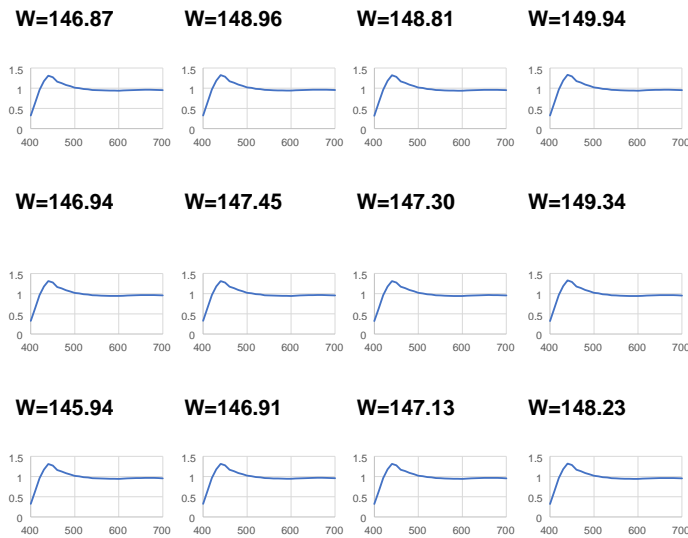
Figure 4.7 Spatial uniformity experiment result.

(a)   (b)
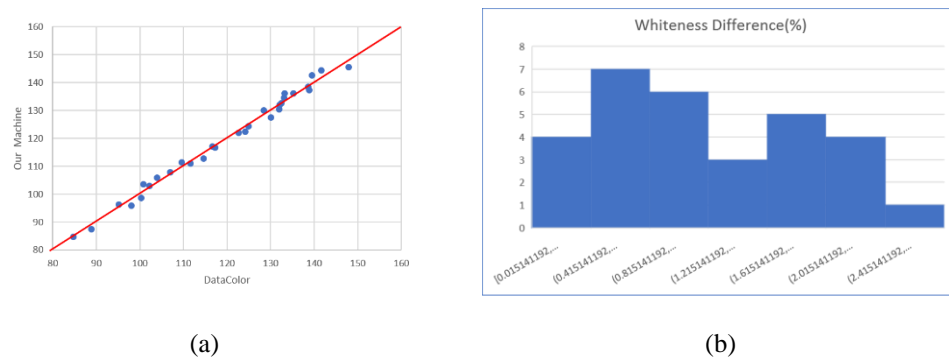
Figure 4.8 Camera response and estimated reflectance under UV100 and UV0. (a)
Camera response. (b) Whiteness difference in percentage.

The result of whiteness measurement experiment is illustrated in Figure 4.8. Figure .4.8 (a) shows the scatter of ground truth and our machine's result. The red line means their number is equal. The scatter are uniformity distribute up and below the red line which means the measurement from our machine is very close to the ground truth from Datacolor.

47

4.5 Conclusion

In this chapter, we proposed to use MSI device to measure the whiteness of a flat object which is especially useful for textile and paper production. In order to conduct measurement, a multispectral imaging system is built by integrating with Xenon light and an integral sphere. Different from the ordinary multispectral imaging system for fidelity whiteness reproduction only for pure reflective materials, this machine can reconstruct the spectral surface for objects which FWAs. To achieve that, the conventional Tungsten is replaced by an Xenon light with integrating sphere. Besides, a UV light box with two filters is designed to simulate two light sources. A linear combination method is extended to combine images under two light sources. At last, a theoretical model is build can applied to whiteness measuring process in the multispectral machine, which ensures the spatial uniformity. The results show the well accuracy and Spatial uniformity for whiteness measurement.

Chapter 5 Automatic classification of knitted fabric textile based on Bag-Of-Words (BoW) and K-Nearest-Neighbour (KNN) Algorithms

5.1 Introduction

Knitted fabric has the characteristic of having well-defined structures (Lv & Long, 2015). In handling kintted fabric, it is often difficult to distinguish between different kinds of structures and hence negatively affect the quality control process. Manual inspection of weft knitted stitch has significant shortcomings such as labour intensive, low accuracy and time consuming. It is therefore desirable to apply computer vision techniques and imaging devices to recognize the patterns and structures of knitted fabrics.

Automatic inspection of yarn-dyed fabric has attracted research attention for many years (C. F. J. Kuo & Kao, 2007; Pan et al., 2010). However, there are little work in automatic recognition of knitted fabric. Because 1) there are much more structures of knitted fabrics than yarn-dyed fabrics; and 2) The knitted fabrics are more flexible than yarn-dyed fabrics which make it very difficult to perform yarn segmentation. Yarn segmentation is an important step in the recognition process to identify each individual yarn in the fabric.

The inspection of knitted fabric has changed from the direct recognition to classification(Lv & Long, 2015). That means in the database there are a lot of knitted fabric samples in various categories. When there is a new knitted fabric, the objective is to assign a predicted category to the fabric.

In this chapter, the methods to classify the structure of knitted fabrics based on digital images are reviewed and examined. A new feature extraction method based on global features is also proposed. Using the new method, the classification accuracy of knitted fabrics can be significantly improved. In the experiment, 290 knitted fabrics with 58 different textures and 5 different colours are involved. The result shows that the proposed method is superior to the current state-of-the-art method in terms of classification accuracy.

5.2 Related works

In this section, the work of yarn-dyed fabric recognition is introduced and the reason why the method cannot be used in knitted fabric inspection is explained. Several work of the knitted fabric classification will also be introduced.

Conventional yarn-dyed fabric classification often includes angle correction, directional projection, yarn segmentation and float point classification (C. F. J. Kuo et al., 2004; Pan et al., 2010; B. J. Xin et al., 2009; B. G. Xu, 1996; J. Zhang et al., 2018). However, for knitted fabric, yarn segmentation is highly difficult because the yarns are more flexible than they are in the yarn-dyed fabrics.

Although not many, there are two literature directly related to the work of knitted fabric classification. Tang-jun Lv and Hai-ru Long have applied the SURF algorithm to knitted fabric classification and recognition (Lv & Long, 2015). They first applied Gaussian denoise and then select the local feature. They make use of the reparability of patterns in the same fabric and use the SURF feature to match these patterns. Kuo and Kao have used the co-occurrence feature and SMO (self-organizing map) network to

classify the knitted fabrics (C. F. J. Kuo & Kao, 2007). The disadvantage of co-occurrence feature is that it can only detect a small number of classes. For example, in Kuo and Kao's work, there are only 5 classes which are plain weave, twill weave, stain weave, single jersey, double jersey, and non-woven fabric.

In the proposed work, a larger dataset is build and made publicly available. The most popular image classification methods are tested with the proposed the global feature method. Researchers working in the same field can verify the algorithms and methods in the dataset.

5.3 Classification Method

A traditional classification task can be depicted in Figure 5.1. It consists of two parts: the training phase (left) and the testing phase (right).

The detailed steps are:

1. Datasets are separated as training dataset and testing dataset.
2. Features are extracted on each training sample and stored in the feature database.
3. Feature database are used as input to train a classification model.
4. Each testing sample is selected for feature extraction.
5. Use feature extraction method to extract the feature vector of the testing sample.
6. Use the trained classification model to predict the category of the testing sample.

From the above steps, the knitted fabric classification task involves two key processes, they are feature extraction and data classification. The following passages summarizes existing techniques for the two key processes.
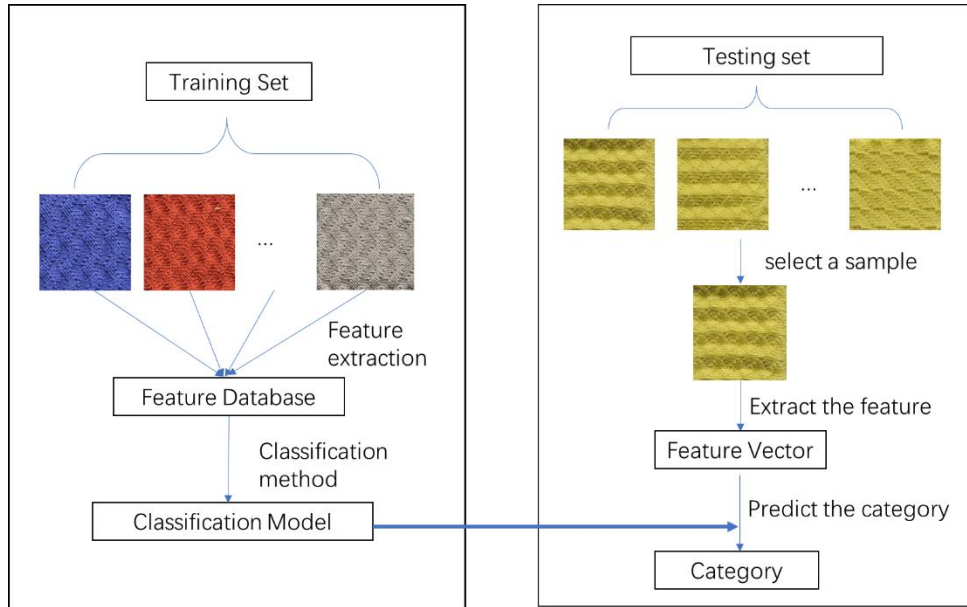
Figure 5.1 Decomposition of the image classification task

Grey level co-occurrence matrix (GLCM) is a popular method for texture analysis, it estimates image properties related to second-order statistics (Raheja, Kumar, & Chaudhary, 2013; Zhu, Pan, Gao, & Zhang, 2015). It defines a distribution of co-occurring pixel values (greyscale values, or colours) at a given offset. After the matrix is build, many physical properties can be obtained using the matrix. In this work, similar setting as KJ KUO(C. F. J. Kuo & Kao, 2007) including contrast, entropy, uniformity (also called energy) and homogeneity are used for GLCM.

GIST descriptor is a popular techqniue in feature extraction (Oliva & Torralba, 2001). It is based on a low dimensional representation of the scene which is called Spatial Envelope. Bag of Word (BoW) is another feature extraction method from the literature in natural language processing (NLP) (Sivic & Zisserman, 2008). The advantage of the BoW is that the models are invariant to image translation, scaling, and rotation, partially invariant to illumination changes and robust to local geometric distortion (Csurka, Dance, Fan, Willamowski, & Bray, 2004; Nowak, Jurie, & Triggs, 2006).

The two main BOW feature extraction models implemented in the fabric image retrieval system are Scale-Invariant Feature Transform (SIFT), Speeded Up Robust Features (SURF). In the SIFT model (Lowe, 2004), the key-points are defined as maxima and minima of difference-of-Gaussian functions applied in scale space to a series of smoothed and resampled images. SURF detects points of interest in an image in a multi-resolution representation. The standard version of SURF is several times faster than SIFT and is claimed to be more robust than SIFT (Bay, Tuytelaars, & Van Gool, 2006).

Finally, Support VectorMachine (SVM) (Bishop, 2006; Scholkopf & Smola, 2001) and K-nearest-neighbor (KNN) (Bishop, 2006) are two widely used classification methods in machine learning and computer vision. SVM is often used in large scale image retrieval and KNN is often used in comparatively small dataset.
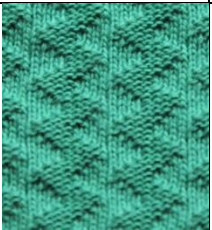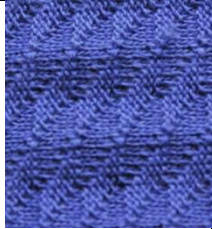
5.4 Experiments

5.4.1 Data

Physical knitted fabrics are fabricated by the Shima Seiki knitting machine, with 5 colour centers including grey, red, green, yellow and blue and 58 texture structures are knitted for each colour center. These texture structures are representative of the commonly used ones by the knitwear industry. The images are acquired in a VeriVide light cabinet and using a Nikon D300 DSLR camera with 450 DPI (Dot Per Inch) resolution.

Images are captured in the form of RAW data, which can provide more information then compressed JPEG files. The obtained RAW data is first converted to DNG format and then finally to RGB image with the procedure outlined in (Can Karaimer & Brown, 2018; Sumner, 2014). Figure 5.2 shows some examples of the knitted fabrics.

Table 5.1 Examples of the knitted fabric samples

Blue	Red	Grey	Green	Yellow

MATLAB is used as the software tool to develop this work. There are 58 textures (structures) and each structure can be viewed as a class. The process is to select some of the samples as training set and the remaining as testing set. There are four sets of experiments in this work show that our proposed method is better than the existing ones. The difference between the four experiments is the method to divide the training set and the testing set.

Experiment 1: Sample of 4 specific colours in each texture is used as a training set, and the remaining one colour is used as a test set. The purpose is to verify the performance of the algorithm when the colour is not included in the testing set.

Experiment 2: Randomly select 4 samples from 5 samples of each texture as testing set, in this setting, the colour of the testing set is likely to appear in the training set also.

Experiment 3: Three specific samples in each texture are selected as the training set, and the remaining two colours were used as test sets. In our experiment, we chose blue, red and grey samples as the training set.

55

Experiment 4: Samples of 3 random colours in each texture are used as training set, and the remaining two colours are used as test sets.

By comparing Experiments 1 and 2 / Experiments 3 and 4, the training samples' effect on the result can be obtained. In contrast, by comparing Experiments 1 and 3 / Experiments 2 and 4, the training colours' effect on the result can be obtained.

5.4.2 Results Analysis

The results of the experiments are measured by accuracy as forumulated below:

Accuracy = No. of samples correctly classified / Total no. of samples

Table 5.2 shows the performance of the implemented classification models described in Section 5.3, applied to the images in the dataset.

Table 5.2 Accuracy for different methods in the 4 experimental settings. The maximum accuracy of each experiment is highlighted.

	Exp 1	Exp 2	Exp 3	Exp 4
BoW +SIFT +SVM	0.5345	0.5439	**0.5862**	**0.5948**
BoW +SURF + SVM	0.6034	0.5614	0.5603	0.5431
BoW +SIFT +KNN	**0.6207**	0.5789	0.5439	0.5776
BoW +SURF + KNN	0.5000	**0.6491**	0.5690	0.5862
GIST + SVM	0.2931	0.3509	0.4052	0.2845
GIST+ KNN	0.3448	0.4035	0.3707	0.3448
GLMC +SVM	0.0172	0.0175	0.0172	0.0172

GLMC+ KNN	0.0517	0.0351	0.0431	0.0259

From the results, the BoW feature extractor has better performance over the GIST and GLMC. Moreover, it can be seen that the classification method has limited effect on the final retrieval result. The highest accuracy of each experiments is appeared in feature extraction method BoW.

Table 5.3 total accuracy for 4 experiments

	Exp 1	Exp 2	Exp 3	Exp 4
Average BoW accuracy	0.56465	0.583325	0.56485	0.575425

The accuracy of 4 BoW methods of Table 5.2 are averaged and shown in Table 5.3. The correctness of 4 colour is nearly the same as the random 4 training colour while the 3-training colour is larger than the random 3 training colour. That means when the colour is unseen in the database (training set), the performance is still robust.

Besides, when using 4 colours as training, the result is worse than when using 3 colour as training, but the random 4 colour training is better than the random 3 colour training, that means, the training data will not change the results too much.

Table 5.4 total accuracy for 6 methods

BoW +SIFT + SVM	BoW +SURF + SVM	BoW +SIFT + KNN	BoW +SURF + KNN	GIST + SVM	GIST+ KNN

2.2594	2.2682	2.3211	2.3043	1.3337	1.4638

Next, the performance of KNN classification and SVM classification method are compared. we will find we the extract method is BoW, the results are nearly the same, but when the extract method is GIST, KNN has better performance. From above analysis, the KNN method can catch equal performance as the SVM. When the training data is limited, the KNN method is more recommended due to its efficiency advantage.

Categories effect

Table 5.5 the effect of categories

Method/Categories number	10	20	30	40	50
BOW + SIFT +SVM	0.6	0.55	0.4667	0.55	0.54
BOW +SURF + KNN	0.9	0.55	0.4667	0.525	0.58
BOW + SIFT +KNN	0.6	0.55	0.5	0.55	0.5
BOW +SURF + KNN	0.9	0.55	0.4667	0.525	0.58
GIST + SVM	0.5	0.4	0.3333	0.325	0.34
GIST+ KNN	0.7	0.55	0.4	0.4	0.4
GLMC +SVM	0.1	0.05	0.0333	0.05	0.02
GLMC+ KNN	0.5	0.25	0.1667	0.125	0.14

Intuitively, the number of categories will have a large effect on the final results. But to the best of our knowledge, the current literature only involves a small number of categories. In our experiment, we randomly selected 10, 20, 30 ,40 and 50 categories from our 58 categories samples for evaluation of the effect of categories effect. Then 6 methods are applied to test the accuracy.

We can find the method BoW is robust with the increasing of the categories and each of the accuracy keeps stable with the increasing of the category numbers. The GLMC method with the KNN classification method changes most dramatically with the change of the category number. The GIST method with the KNN is more stable than the GIST with SVM.

Time analysis

The experimental environment is detailed as following: the CPU of the machine is Intel i7-8700K, with Toshiba 256G SSD and 2T Hard Disk for store data. The memory is 16G.

Table5.6 Time consuming of all kinds of method with Unit second.

BoW +SIFT + SVM	BoW +SIFT+ KNN	BoW +SURF+ SVM	BoW +SURF + KNN	GIST + SVM	GIST+ KNN	Grey +SVM	Grey + KNN
50.74	4.76	22.35	4.56	23.84	7.31	23.00	1.32

Due to the results differs a little in accuracy, in the time analysis part, we only test the Experiment 1 (4 same colour as training). There are 58 samples tested. Comparing to methods GIST and GLMC, the BOW needs a lot of time for clustering(k-means). But, when we acquire an enquire, the clustering will not affect the costing time. Therefore, in our results, we will not count in the clustering time cost. Comparing to classification KNN, SVM need more time in training part. In consideration of their nearly equal performance, KNN is obviously more suitable for this work.

From the table, the GLMC requires the least running time, since it is very easy in feature extraction. However, the performance in accuracy is sub-optimal. Form the time cost table, it shows that the SVM classification consistently cost more time than KNN method.

5.5 Conclusion

To conclude, a recognition method for knitted fabric structure based on bag of virtual words is proposed. In this work, the common methods in classification for knitted fabric textile are investigated. The KNN classification method cost less time in the experiment. In the future, more complicated scenario should be explored. For example, performing image retrieval of knitted fabrics. Moreover, since the data and codes are released online, researchers can easily re-implement and evaluate the proposed work. After that, they can propose their algorithms to boost the research in fabric automatic inspection.

Chapter 6 Automatic colour pattern recognition of multicolour printed fabrics using multispectral image system

6.1 Introduction

Printed fabrics and other valuable textile materials have rich colours and variable patterns. Besides the fabric structural parameters (such as fabric densities, weave pattern), the colour pattern of printed fabrics is the most significant feature, which can be described by the number of colours, colour values, and patterns. Many researches have been done to measure fabric densities(Liu et al., 2014; Schneider et al., 2014; J. Zhang et al., 2014) and recognize weave pattern(Li et al., 2020; Wang et al., 2011). To the best of our knowledge, it is the first attempt to recognize colour pattern and measure fabric colours of printed fabrics by using multispectral image system.

The colour pattern recognition is indispensable for the textile and dying industries, including colour measurement and pattern segmentation, when reproducing the clients' standard samples or controlling the quality of the batch fabrics in production. Compared with manual colour pattern inspection, the automatic recognition method based on computer vision is more desirable to improve manufacturing efficiency and reduce the labour costs.

For accurate colour measurement, it is necessary to obtain the spectral reflectance of the object surface, as shown in Figure 6.1(c) and (d). The colour values under different light sources (e.g., Daylight, CWF, etc.) can be calculated from the spectral reflectance curve. Traditionally, the spectral reflectance curve of object colour can be obtained by

61

spectrophotometer, like DataColor. It can measure the average reflectance of a limited area accurately, thereby only suitable for solid-colour fabrics. However, it cannot capture the image of the object surface and measure colours in any multicoloured object. Although the common industrial cameras are trichromatic rather than multispectral, thereby capturing the RGB image of the object surface. However, it cannot obtain the spectral reflectance information of the object so that the measured colours are not accurate for industrial standard.

Multispectral imaging (MSI) system is developed that has the potential to measure the colours of a multicolour printed fabric. Compared with a spectrophotometer, a MSI system can provide not only the spectral information but also the spatial information of a multicolour fabric. The MSI can recover multispectral reflectance from 16 grey-scaled images captured by a monochrome camera with sequentially placing band-pass filters of various wavelengths, across the visible spectrum (i.e., 400 -700 nm) for every pixel in the image. The MSI can obtain the spectral reflectance of an object and hence it can provide colours under any known light source, such as D65, A, CWF, etc. The LAB image in the uniform CIE (1976) L*a*b* colour space can be converted from the multispectral image for further colour extraction and pattern segmentation.
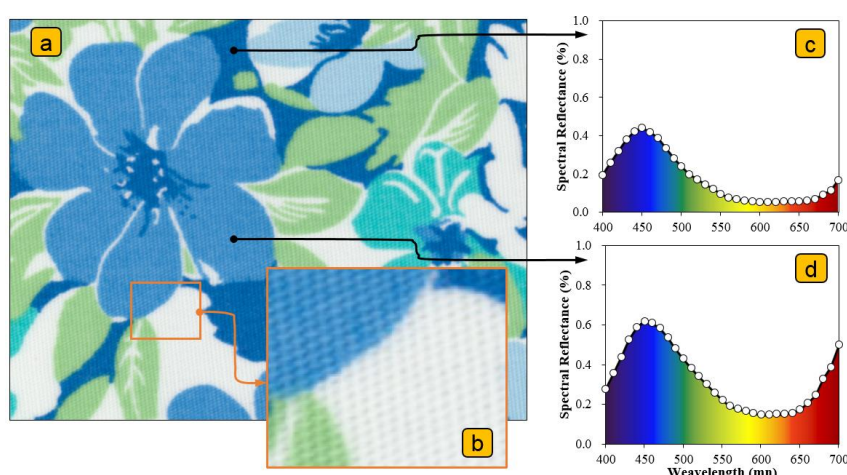

Figure 6.1 Illustration of multicolour printed fabric sample.

62

(a) The captured multispectral printed fabric image. (b) The magnified local region with clear texture. (c) The spectral reflectance curve of one dark blue pixel. (d) The spectral reflectance curve of one light blue pixel.

The previous studies (C.-F. J. Kuo & Kao, 2008; C.-F. J. Kuo & Shih, 2011; C. F. J. Kuo, Kao, & Chiu, 2009; C. F. J. Kuo, Shih, Kao, & Lee, 2005; C. F. J. Kuo, Shih, & Lee, 2008; Mo, Xu, Ouyang, & Wang, 2017; Ouyang, Xu, & Yuan, 2019) mainly focus on the colour extraction and pattern segmentation of RGB printed fabric image that have two main steps: (1) Colour clustering, (2) Pattern segmentation. Usually, the pattern segmentation of fabric image can be realized easily after the colour clustering and extraction in a colour pattern recognition system. They adopt fuzzy c-means (FCM) clustering method(C.-F. J. Kuo & Shih, 2011; C. F. J. Kuo et al., 2005; C. F. J. Kuo et al., 2008) or self-organizing-map (SOM) based clustering algorithm (C.-F. J. Kuo & Kao, 2008; C. F. J. Kuo et al., 2009; Mo et al., 2017; Ouyang et al., 2019) to cluster the colour pixels directly. However, there are four main factors affecting the performance of colour clustering and extraction.

1. Uneven colour distribution. It is because of the surface texture and yarn structure of the printed fabric, as shown in Figure 6.1(b). The sections of yarns in the fabrics are in the form of elliptical shape. The pixels in the interstices and intersection between yarns have lower grey levels, whereas the colour pixels around the centre of the warp and weft yarns possess higher grey levels. Furthermore, the colours on the regional boundaries are affected by the neighboring colour regions interdependently.

2. Adjacent colour. Some printed fabrics have similar adjacent colours whose colour difference is small in the CIELAB colour space, this makes it harder to separate and extract them by using clustering method. For example, there are three blues in Figure 6.1: dark blue (Figure 6.1(c)), light blue (Figure 6.1(d)) and baby light.

3. Unequal colour percentages. Some printed fabrics have intricate pattern whose colours have different percentage, colours with small percentages are tend to be ignored by the clustering algorithm.

4. Light Transmission of fabric. The printed fabrics with small fabric densities have high transmission of light, in which the platform colour will affect the captured image and results in inaccurate colour measurement of the fabric.

Previous studies do not take these factors into consideration. An image filter should be used to remove noise to mitigate the influences of Factor 1 and 4. They adopt the clustering method to process the fabric image directly and do not filter the captured image at the beginning. Besides, FCM clustering method is a kind of partitional clustering method which applies the same weight to all the points in the data set (Xiao & Yu, 2012). Moreover, Factor 2 and 3 cannot be solved with the FCM clustering method. SOM dose not perform well in cases which are affected by the number of variables for the nonoverlapping cases (Mingoti & Lima, 2006), thereby it is also hard to deal with Factor 2 and 3. The computing time is also important for the practical application. However, the SOM computation is time-consuming because of many nodes is used. Furthermore, these methods are just used and tested for traditional 3-channel RGB colour images, not the high-dimensional multispectral images.

During the multispectral image processing, the colour image in CIELAB colour space is converted from the multispectral image and three features of each pixel are calculated by applying principal component analysis to reduce the dimensions of the multispectral image. The noise pixels are removed by calculating the local stability of each pixel firstly, and then the rest stable pixels are clustered by the proposed grid-based density peaks clustering (GDPC) algorithm based on the

6.2 Machine Vision Algorithms

6.2.1 Multispectral Image Transformation

After capturing and reconstructing the multispectral data of the fabric sample, the multispectral data should be transformed into the X, Y and Z tristimulus values and then the L*a*b* values (Nyström, 2006). The coordinates of the CIE 1976 (L*a*b*) colour space (CIELAB) are computed using non-linear transformations from the tristimulus XYZ values (Nyström, 2006; Pointer, 1981). Figure 6.2 shows the captured 16 monochrome images under the 16 different wave bands from 400nm to 700nm with the wavelength interval 20 nm by MSI. After spectral reflectance reconstruction and multispectral image transformation, the fabric images of three channels in CIELAB colour space are illustrated in Figure 6.3.
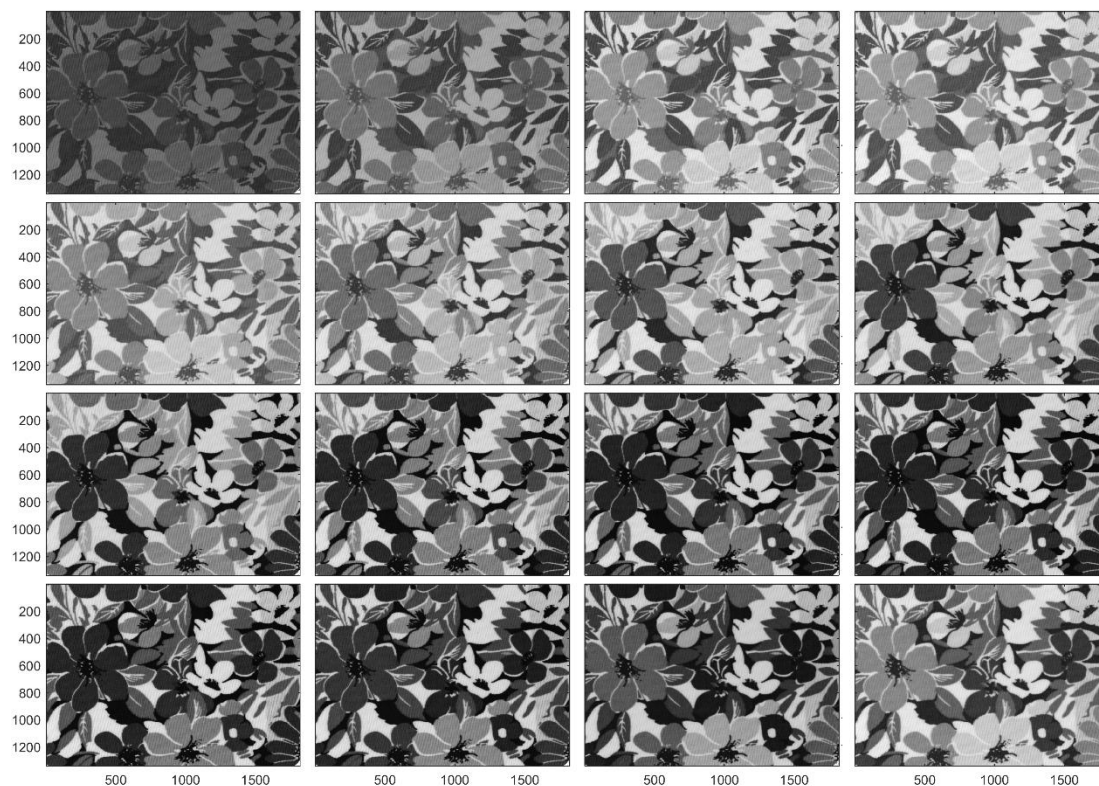

Figure 6.2. The directly captured 16 monochrome images under the 16 different wave bands from 400nm to 700nm with the wavelength interval 20 nm. The wave band increases from the left to the right and from the top to the bottom.
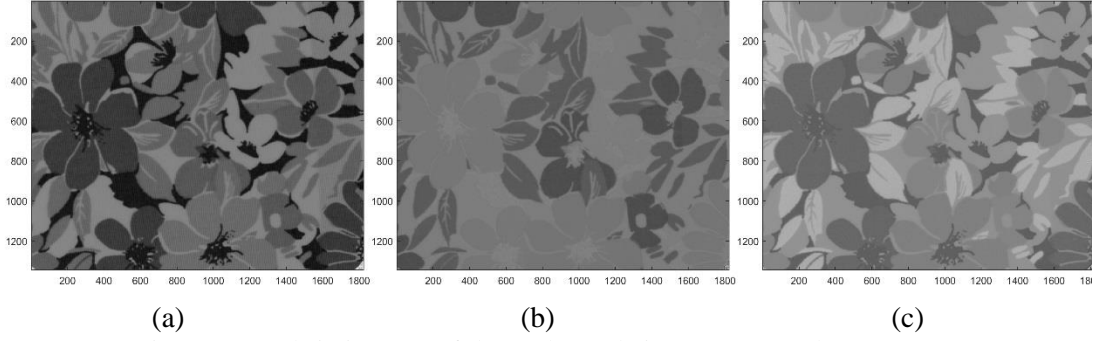
(a)   (b)   (c)

Figure 6.3 Fabric images of three channels in CIELAB colour space.
$L*$. (b) $a*$. (c) $b*$.

6.2.2 Colour Image Filtering

There are shaded areas in the interstices and intersection between yarns. Furthermore, the colours on the regional boundaries are affected by the neighbor colour regions interactively. These areal pixels reduce the precise of colour measurement, and therefore affect the performance of colour clustering. It is necessary to use an image filter to remove noise to mitigate these influences based on the pixel colour and spatial information. Meanwhile, the image filter should be designed to not change the original pixel colour values. A stable index S is developed as a pixel selector to filter the noise and save the stable colour, as shown in Equation (6.1). $S_{i,j}$ is the average of the Euclidean distance between the centre pixel and the neighbor four pixels.

$$S_{i,j} = \frac{1}{4} \sum_{m=-1}^{1} \sum_{n=-1}^{1} d(P_{i,j}, P_{i+m,j+n})$$

(6.1)

where $d(P_{i,j}, P_{i+m,j+n})$ is the Euclidean distance between the center pixel $P_{i,j}$ and the neighbor pixel $P_{i+m,j+n}$ in CIELAB colour space, $i=1,2,..,H$ (H is the height of the fabric image), $j=1,2,…,W$ (W is the width of the fabric image), $m=-1,1$, and $n=-1,1$.

The heatmap of the stable index S is shown in Figure 6.4(a). The more smaller the stable index $S_{i,j}$ is, the more stable the stable index $S_{i,j}$ is. The pixels with the lager stable index can be considered as noise and should be remove for future colour clustering. A threshold T_s is a parameter to separate the noise and stable pixels (T_s is set as 2 in the experiment). The filtered fabric image is shown in Figure 6.4(b). Most of pixels in the regional boundaries and yarn interstices are inspected as the noise shown as the black pixels.

The L*, a* and b* values of all pixels in the fabric sample image are shown in Figure 6.5(a) which is mixed and hard to distinguish different colour clusters. By contrast, these values of the saved stable pixels are shown in Figure 6.5(b) after image filtering where the different colour clusters are separated and easier to distinguish them.

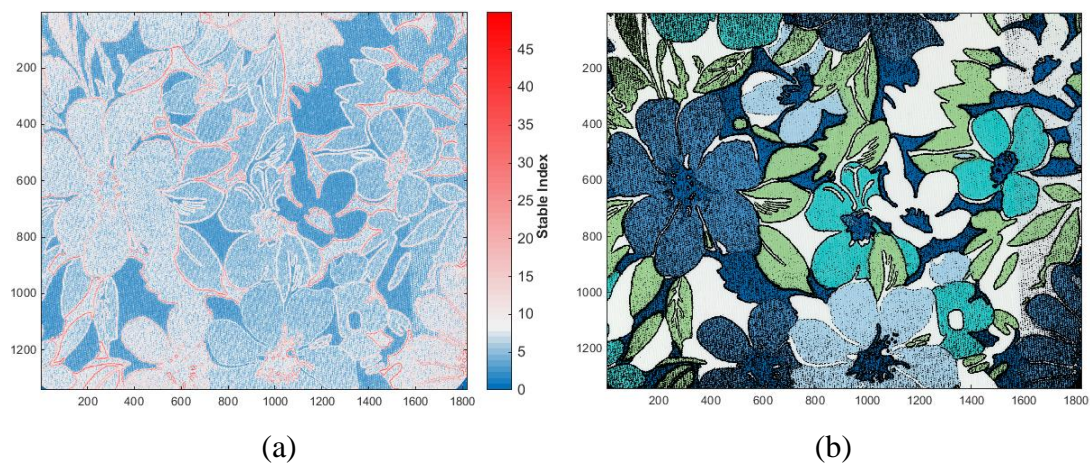(a)   (b)

Figure 6.4 Colour image filtering process. (a) Stable index heatmap. (b) Filtered fabric image.
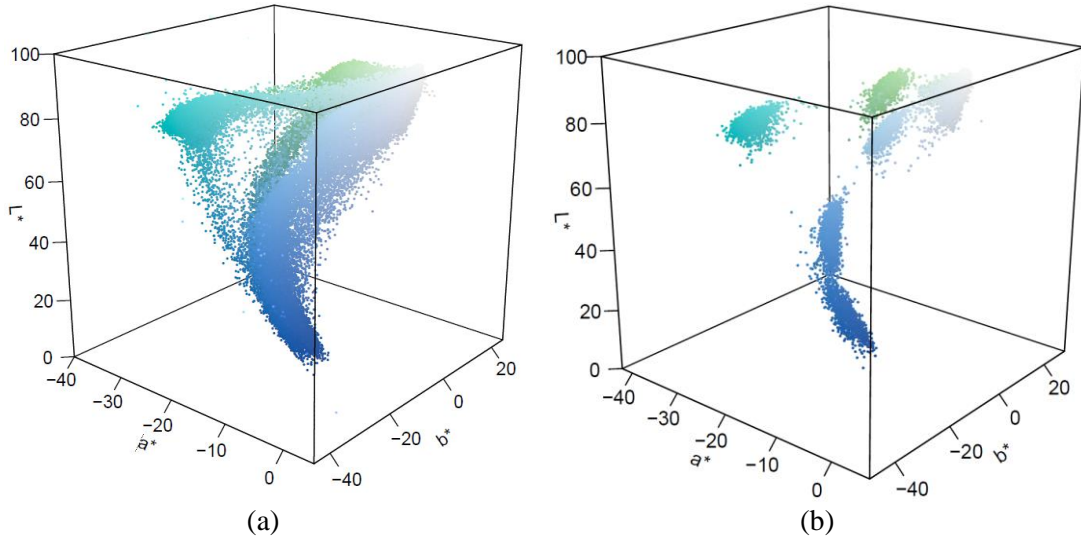
Figure 6.5 Colour distribution. (a) Before image filtering. (b) After image filtering.

6.2.3 Multispectral Feature Reduction

The previous studies demonstrate that it is beneficial and efficient to use the principal component analysis (PCA) technique(Bishop, 2006) as a pre-processing step for the classification of multispectral images(Rodarmel & Shan, 2002). The principal component analysis is based on the fact that neighboring bands of multispectral images (shown in Figure 6.2) are highly correlated and often convey almost the same information about the object. Three multispectral principal features can be extracted by using PCA method, as shown in Figure 6.6. The cumulative proportion of principal component (PC) 1, 2 and 3 are 0.867, 0.963 and 0.992.
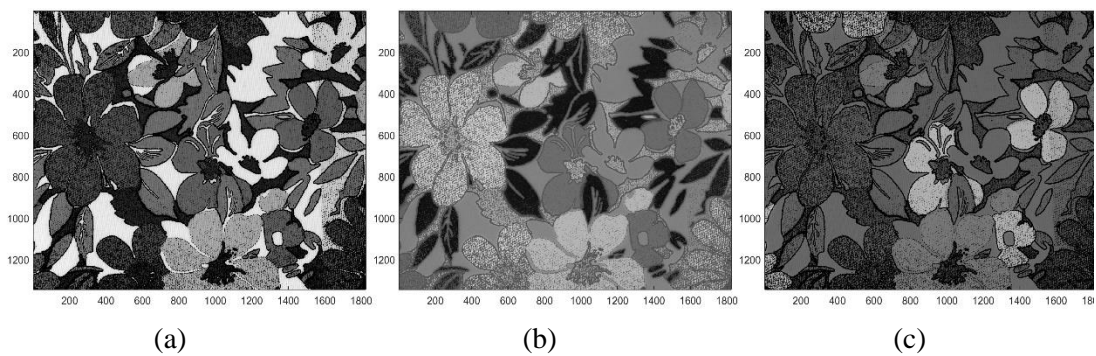

Figure 6.6 Fabric images of three multispectral PCs.
(a) PC1. (b) PC2. (c) PC3.

6.2.4 Colour Pxiel Clustering

The stable pixels are clustered by a grid-based density peaks clustering (GDPC) algorithm based on the CIELAB colour values and three reduced features. Density peaks clustering algorithm (DPC) is proposed by Rodriguez and Laio (Rodriguez & Laio, 2014) and it takes advantage of density and delta-distance to find clustering centers, and then assigns remaining other examples. Compared with the classical algorithms (K-means algorithm(Xiao & Yu, 2012), Fuzzy C-means (FCM) algorithm (Bezdek, 2013) and Spectral clustering (SC)(Ng, Jordan, & Weiss, 2002)) , it is efficient and robust with only one input parameter and does not require the cluster numbers (Cheng, Liu, Huang, & Cheng, 2016). However, it computes the local density by calculating the distance between all points, leading to high computational complexity, especially for the large-scale data set (Guo, Lin, Guo, & Liu, 2016; X. Xu, Ding, Du, & Xue, 2018). To overcome this challenge, a grid-based density peaks clustering (GDPC) with a novel distance calculation equation is developed to cluster the large colour pixels. Unlike the previous GDPC (X. Xu et al., 2018), we use a novel distance calculation equation to compute the minimum distance between the point and any other point with higher density based on the L*a*b* colour value and multispectral PCs.

(1) Grid structure creation and cell density caclualtion

The first stage of the GDPC is grid partition based on the idea of CLIQUE algorithm. Only the L*a*b* colour values of the stable pixels are used to partition a 3-dimensional grid. Given an 3-dimensional data set $P=\{P_L, P_a, P_b\}$, where the values of P_L, P_a, P_b range from 0 to 100, -128 to +128, -128 to +128, respectively and the length of T is the number of the stable pixels. Let $S_n=\{P_L \times P_a \times P_b\}$, the Cartesian product of all three

attributes constitutes a three-dimensional data space, and its value interval is 0.5. The three dimensions of the data space is divided into N_L, N_a and N_b equal and disjoint intervals respectively:

$$N_j = 2 \times (\text{ceiling}(\max(P_j)) - \text{floor}(\min(P_j))) \tag{6.2}$$

where, $j=L$, a and b, ceiling(x) and floor(x) are the ceiling and floor integer of x respectively, max(x) and min(x) is the maximum and minimum of x. Each interval is left closed and right open, so the entire data space is divided into $N_L \times N_a \times N_b$ hypercube units, that is the grid cell. The ith stable pixel should be mapped into the $[n_L, n_a, n_b]$ grid cell G:

$$n_{i,j} = \text{ceiling}(2 \times (P_{i,j} - \text{floor}(\min(P_j)))) \tag{6.3}$$

where, $j=L$, a and b, $P_{i,j}$ is the jth L*a*b* component of the ith stable pixel. All of the stable pixels are mapped into the grid cells in sequence:

$$g_{(n_{i,L}-1) \times N_L + (n_{i,a}-1) \times N_a + n_{i,b}} = g_{(n_{i,L}-1) \times N_L + (n_{i,a}-1) \times N_a + n_{i,b}} + 1 \tag{6.4}$$

The colour information of the $[n_L, n_a, n_b]$ grid cell is also recoded in an array C, as the colour features of the grid cell.

Meanwhile, the multispectral PCs are also mapped into the $[n_L, n_a, n_b]$ grid cell as the multispectral features of the grid cell.

$$F_{(n_{i,L}-1) \times N_L + (n_{i,a}-1) \times N_a + n_{i,b}, k} = F_{(n_{i,L}-1) \times N_L + (n_{i,a}-1) \times N_a + n_{i,b}, k} + Q_{i,k} \tag{6.5}$$

where $k=1,2,3$, $Q_{i,k}$ is the kth multispectral principal component of the ith stable pixel. Theoretically, the same colours should have the similar or same multispectral principal components. Finally, the average multispectral PCs of the grid cells are calculated.

$$F_{i,k} = \frac{F_{i,k}}{g_i} \qquad (6.6)$$

The grid cell density g_i is considered as the number of data points that fall into the ith grid cell. If the $g_i = 0$, the grid cell is empty grid cell; if $g_i > 0$, the grid cell is non-empty grid cell. Based on the arrays of g_i, $C_{i,k}$ and $F_{i,k}$ which indicate the density, the position in the 3-dimensional L*a*b* grid and three average multispectral PCs of the grid cell respectively, where $i=1,2,\ldots,M$ (M is the number of non-empty grid cell, $k=1,2,..,3$, the clustering method will be implemented to cluster the grid cells.

(2) Sparse cells remove and Density peaks search

The sparse cells are removed based on the predefined threshold, and the dense cells are sorted according to their densities and identify cluster centers. Let T_u be a density threshold (T_u is set as 5 in the experiment). If the number of points in a cell is less than T_u ($g_i < T_u$), the grid cell is called low cell (sparse cell) and points in a low cell are outliers; otherwise, the grid cell is called high cell (dense cell). A cluster is defined as a maximal set of connected dense grid cells. Additionally, the high cells will cover most points of the data sets. Therefore, the sparse cells are removed, so as to ensure the accuracy of the clustering and reduce the computing time.

The grid cells are sorted according to their density and we should find the grid cell that is the nearest around the ith point.

$$k = \arg\min_{j:g_{j,1}>g_{i,1}}(dc_{ij}) \qquad (6.7)$$

where $dc_{i,j}$ is the Euclidean distance between the grid cell i and j in the 3-dimensional L*a*b* grid:

$$dc_{i,j} = \sqrt{\sum_h \left(C_{i,h} - C_{j,h} \right)^2} \qquad (6.8)$$

If the kth point is the nearest around the ith point, δ_i is measured by computing the comprehensive minimum distance between the i grid cell and any other grid cell with higher density. The comprehensive minimum distance consists of the left part dc and the right part dp. d_C is the Euclidean distance between the grid cell i and k in the 3-dimensional L*a*b* grid, and dp is the Euclidean distance of multispectral PCs between the grid cell i and k.

$$\delta_i = dc_i + \gamma dp_i = \sqrt{\sum_h \left(C_{i,h} - C_{k,h} \right)^2} + \gamma \sqrt{\sum_h \left(F_{i,h} - F_{k,h} \right)^2} \qquad (6.9)$$

where $h=1,2,3$ and γ is the weight of the dp (in this experiment, γ is set as 10 and will discussed in section of the Results and Discussion)), because the dp and dc have different magnitudes and dp is much less than dc. For the g_i grid cell with highest density, it conventionally takes $\delta_i=\max(\delta_j)$. In order to help users to find the correct of colour clusters, the decide index σ_i is defined to associate g_i and δ_i, as:

$$\sigma_i = g_i \, \delta_i \qquad (6.10)$$

The scatter plot of count(g_i)-distance(δ_i) of fabric sample 0 is shown in Figure 6.7. In Figure 6.7(b), the distance ($\delta_i=dc_i$) is calculated just based on the L*a*b* colour distance and the gap between the minimum value (around 4) of cluster centers (indicated by the blue arrow) and the maximum value (around 15) of cluster members (indicated by the red arrow) is about 11. By contrast, in Figure 6.7(a), the distance ($\delta_i=dc_i+\gamma dp_i$) is calculated just based on the L*a*b* colour distance and multispectral PCs and the gap between the minimum value (around 20) of cluster centers (indicated

by the blue arrow) and the maximum value (around 5) of cluster members (indicated by the red arrow) is about 15. The threshold T_δ is set to distinguish the cluster centers and members. When the L*a*b* colour distance and multispectral PCs both are considered when calculating distance(δ_i), it is more robust and easier to find the cluster centers when setting the threshold T_δ.

As a result, the cluster centers are founded as grid cells for which the value of δ_i is anomalously large. After the cluster centers have been found, each remaining grid cell is assigned to the same cluster as its nearest neighbor of higher density, as shown in Figure 6.8(a). Finally, the stable pixels are clustered into six groups, as shown in Figure 6.8(b). The multispectral reflectance of six colours are the means of that of the stable pixels within the same clusters, and the fabric colour values in CIELAB colour space are transformed from the mean multispectral reflectance.
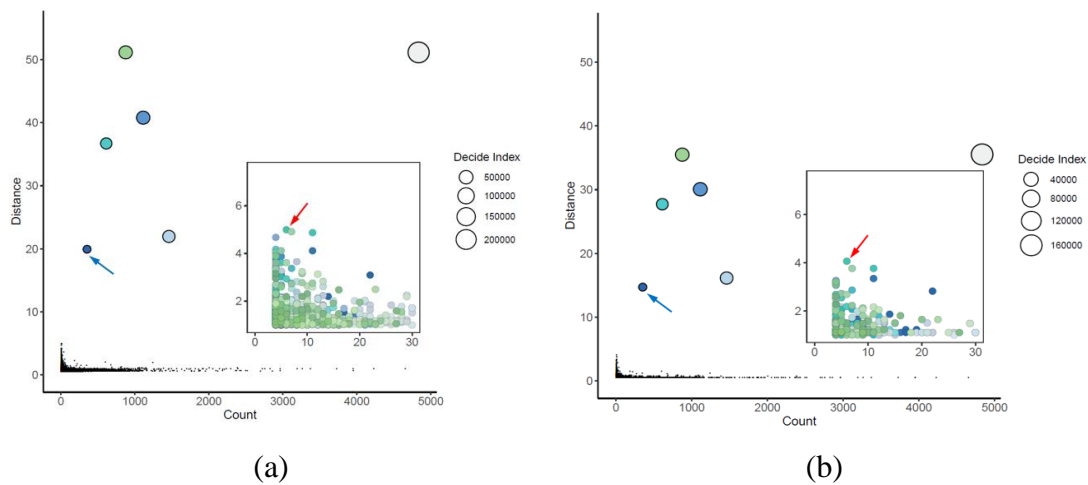

(a)   (b)

Figure 6.7 Decision graph based on different distance(δ_i). (a) *dc+dp*. (b) *dc*.
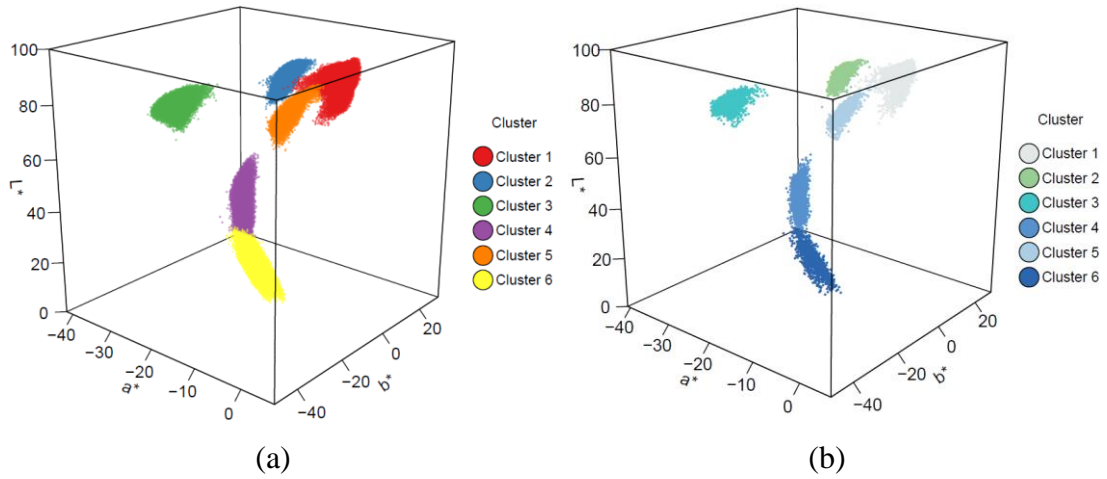
Figure 6.8 Clustering results. (a) Grid cells. (b) Stable pixels.

6.2.5 Colour Pattern Segmentation

Based on the clustering result of the stable pixles, the corresponding colour pattern of the stable pixles is shown in Figure 6.9(a). The k-Nearest Neighbor (KNN) alogrithm (Hastie & Tibshirani, 1996) is used to classify the removed noise pixels based on the grid cells with known colour clusters. The final colour pattern is shown in Figure 6.9(b) and the segmented regions of six colours is shown in Figure 6.10.
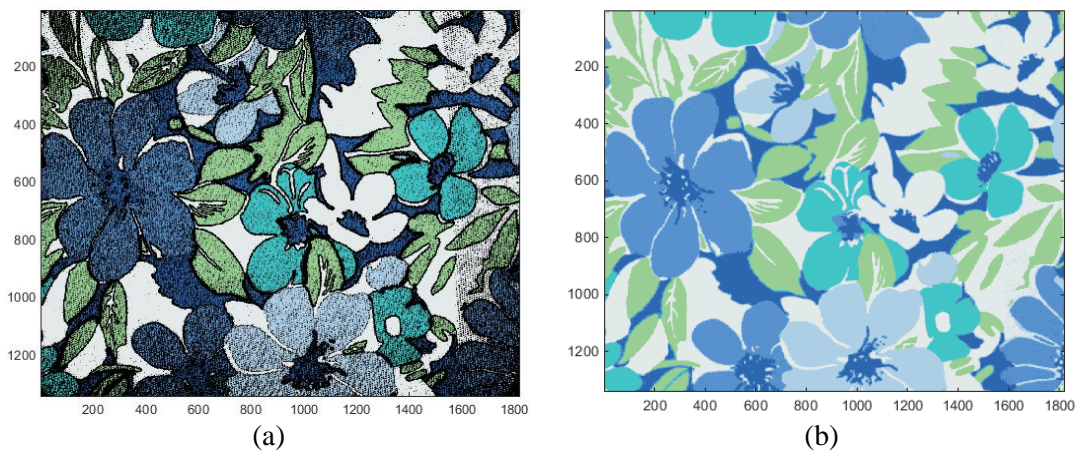
Figure6.9 Colour pattern segmentation result. (a)Colour pattern of the stable pixels. (b) Colour pattern of all colour pixels.
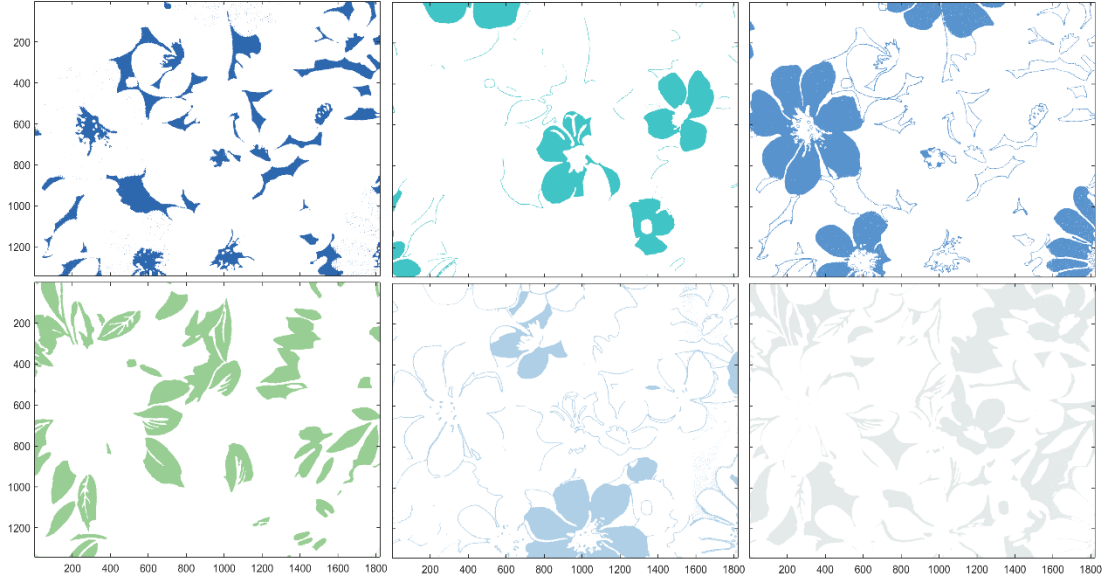
Figure 6.10 Segmented regions of six colours.

6.3 Experimental Results

6.3.1 Algorithmic Parameter Selection

In the proposed method, there are four parameters: a threshold T_s to separate the noise and stable pixels, a threshold T_u to remove the grid cells with small density, a threshold T_δ to distinguish the cluster centers and members and a weight γ in the distance calculation equation $(\delta_i = dc_i + \gamma dp_i)$. The threshold T_s to separate the noise and stable pixels is related to the fabric texture and can be set as [2,4].

Among them, the most important parameters are γ and T_δ. Interestingly, the range selection of T_δ is affected by γ. The optimal γ should meet the requirement that the minimum value of cluster centers (δ_c) is enough big and the maximum value of cluster members (δ_m) is as small as possible, which can make the range selection of T_δ bigger.

75

It is necessary to analyze the range of T_δ when different weight γ are used for different multicolour printed fabrics.
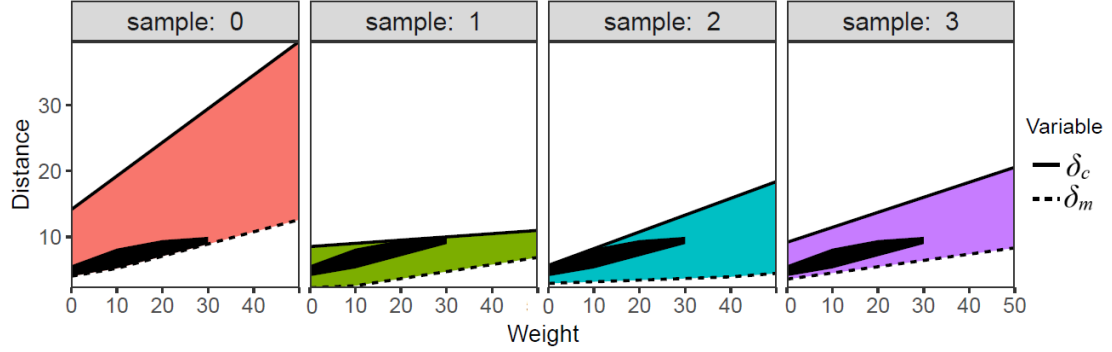

Figure 6.11 The influence of the weight γ for clustering of colour pixels in different fabric samples.
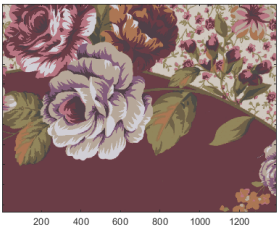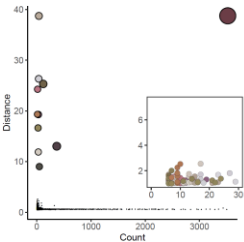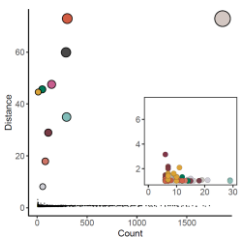
The fabric sample 0,1,2 and 3 are selected to analyze the influence of the weight γ for clustering of colour pixels, as shown in Figure 6.11. The black solid line is the minimum value of cluster centers (δ_c) under different weight γ from 0 to 50 and the black dashed line is the maximum value of cluster members (δ_m). The colour region in each figure is the range of T_δ under different weight γ. The black region is the common region of the T_δ in these four subfigures, which indicates the selected range of γ and the corresponding threshold T_δ to distinguish the cluster centers and members. Figure 6.11 illustrates that when the weight γ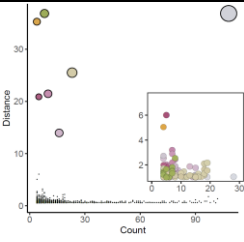 is set as from around 10 to 15, the difference of δ_c and δ_m is bigger and the threshold T_δ can be set as from around 6 to 8.

6.3.2 Datasets and Results

To verify the performance of the proposed method, we performed the experiments on ten images of multicolour printed fabrics with variable patterns and the number of these fabric colours ranges from three to thirteen. The colour pattern recognition results of nine fabric samples are shown in Table 1 and the clearer images can be seen in the appendix.

Based on human vision judgments, it can be found that the recognized colour patterns of sample 1 to 8 are consistent with the physical printed fabrics. The threshold T_s is set as 4 to separate the noise and stable pixels. The threshold T_δ is set as 7.5 in the decision graph and the extracted fabric colours are also illustrated in Table1. However, there are misrecognized red and other colours in recognized colour pattern of fabric sample 9. The fabric sample 9 have rich colours with adjacent colours and intricate pattern with colour lines, which make it hard to extract the colours accurately.

Table 6.1 colour pattern recognition results of different fabric samples.

No.	Original Image	Recognized Colour Pattern	Decision graph	Colours
1				
2				
3				

4			
5			
6			
7			
8			
9			
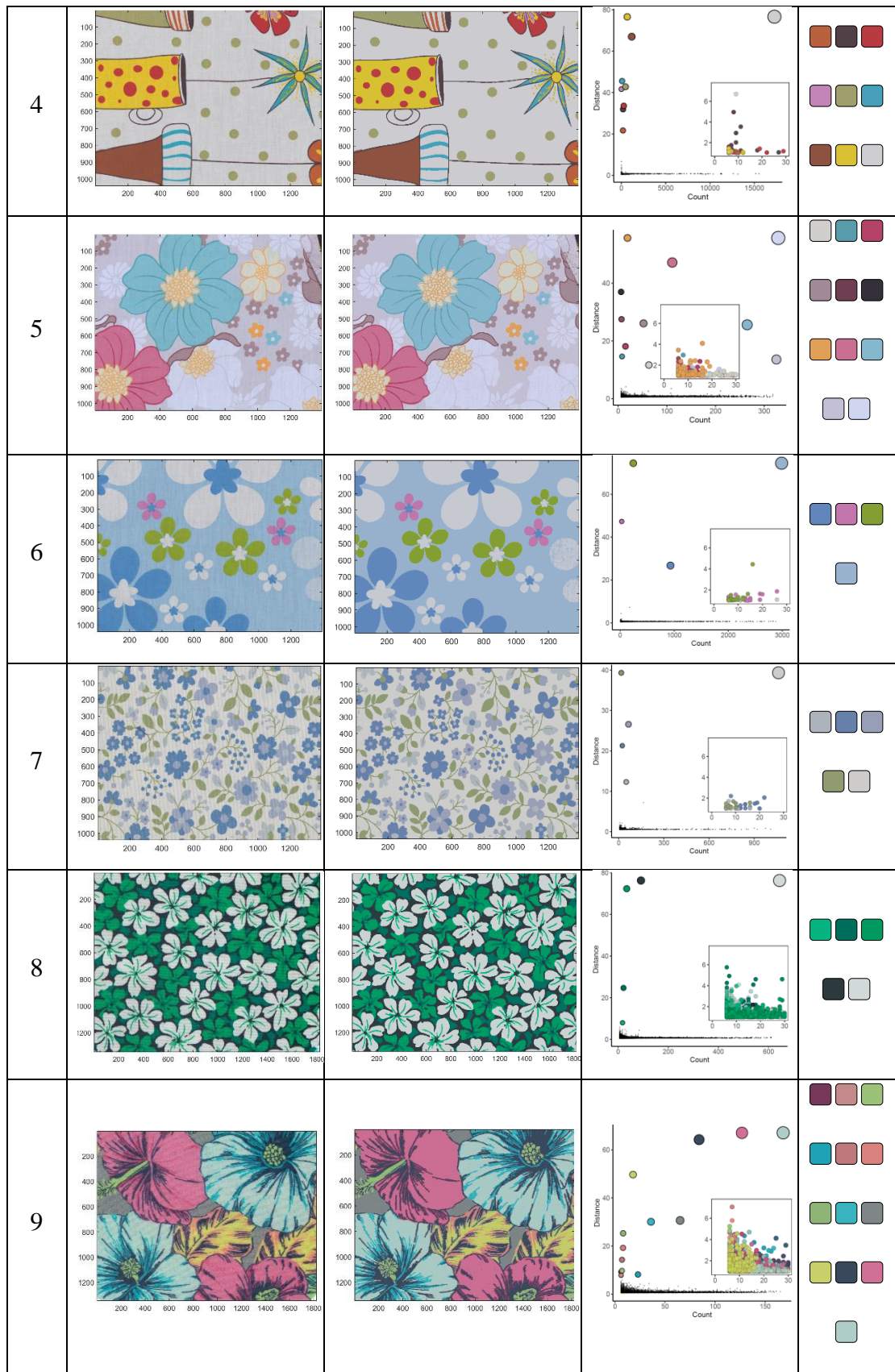
6.3.3 Methods Comparison

We evaluated and compared the colour segmentation results on three fabric images via three unsupervised learning algorithms, including the proposed GDPC, Fuzzy C-means (FCM) algorithm(Bezdek, 2013), and e kernel-based fuzzy c-means (KFCM) algorithm(D.-Q. Zhang & Chen, 2003). Compared with the k-means clustering algorithm based on hard assignment that is not applicable for complex data sets which contain overlapping clusters or contain some data points that cannot be easily assigned to one cluster, FCM algorithm is based on soft assignment and can provide much detailed information about the hidden structure of the data (Xiao & Yu, 2012). However, Since the original FCM uses the squared norm to measure similarity between prototypes and data points, it can only be effective in clustering 'spherical' clusters. By contrast, the KFCM algorithm is robust to noise and outliers and also tolerates unequal sized clusters (D.-Q. Zhang & Chen, 2003). Hence, FCM and KFCM are used to cluster the stable pixels after the colour image filtering to make comparison of segmentation performance with GDCP. In the KFCM algorithm, the Gaussian function is selected as a kernel function i.e. $K(x,y)=\exp(-\|x-y\|^2/\sigma^2)$ and the σ is set as 150. The maximum iterations of FCM and KFCM clustering algorithms is set as 100 and 200 respectivley.

In addition to the human vision judgment, the peak signal-to-noise ratio (PSNR) (Chang, Xu, Xiao, & Srikanthan, 2005; Kanjanawanishkul & Uyyanonvara, 2005) of the segmented colour pattern image is used to assess segmentation performance of multicolour printed fabrics. The PSNR is defined as follows:

$$PSNR = 10\log\left(\frac{Max(Original\ Image)^2}{MSE}\right) \qquad (6.11)$$

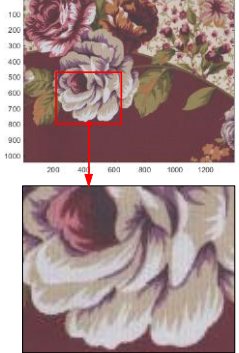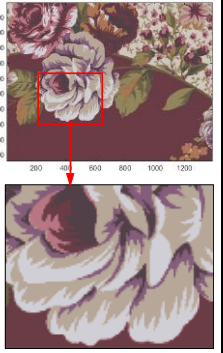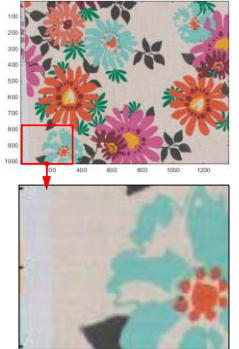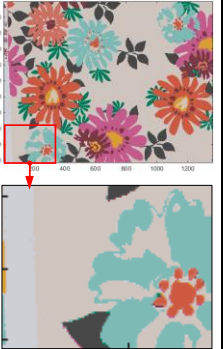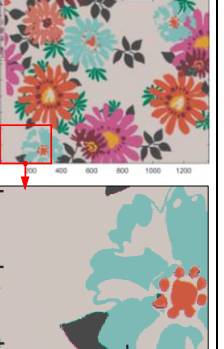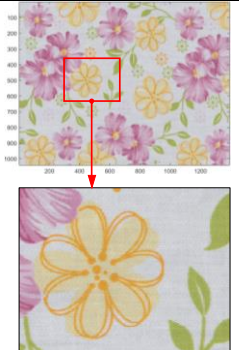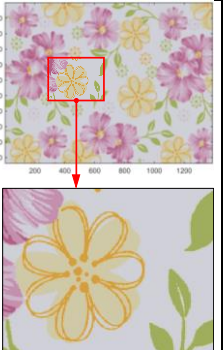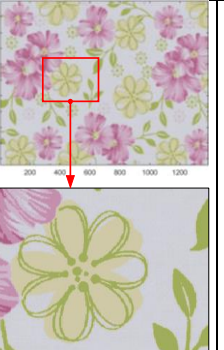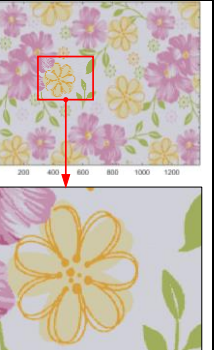$$MSE = \frac{\left(\sum_{j=1}^{N_t} \left(X_j - X_j' \right)^2 \right)}{N_t}$$

<div align="right">(6.12)</div>

where X_j and X_j' indicate the pixel values of the original and quantized image, and N_t is the total number of pixels. In three-dimensional spaces (RGB), Max(Original Image) is equal to $\sqrt{255^2 + 255^2 + 255^2}$. The higher the PSNR value, the higher similarity between the original fabric image and the reconstructed colour pattern image. PSNR is a good measure for comparing restoration results for the same image, but between-image comparisons of PSNR are meaningless (Kanjanawanishkul & Uyyanonvara, 2005). The colour pattern recognition results of fabric samples by using different clustering algorithms are shown in Table 2.

In Table 6.2, for fabric sample 1, the purple in the region of flower is misrecognized as the dark red by FCM and KFCM algorithms; furthermore, the white in the region of flower is misrecognized as the light grey by FCM algorithm. For fabric sample 2, the white region in the left and bottom is misrecognized as the grey red by FCM and KFCM algorithms, because there two similar colours (white and grey) with significantly different amount. For fabric sample 3, the yellow in the flower profile is misrecognized as the green by FCM algorithm. Besides, the PSNR values of the proposed GDPC in three fabric samples are larger than that of FCM and KFCM algorithms. The experimental results demonstrate that the proposed GDPC algorithm can recognize colour pattern from more intricate multispectral images with higher precise, compared with FCM and KFCM algorithms.

Table 6.2 Colour pattern recognition results of different clustering algorithms.

No.	Original Image	Ours	FCM	KFCM

1			
t (s)	-	15.36	139.59	207.72
PSNR	-	68.81	65.23	65.68
2			
t (s)	-	11.18	127.20	226.25
PSNR	-	62.62	62.32	62.40
3			
t (s)	-	12.41	79.70	199.45
PSNR	-	65.89	61.99	63.35

The time complexities of FCM, KFCM, DPC and GDPC are $O(nK^2i)$, $O(n^2Ki)$, $O(n^2)$ and $O(n)+ O(m^2)$ respectively, where, n is the number of data points, i is the number of

iterations and K is the number of clusters. m is the number of nonempty grid cells, compared to the number of data points is very small. In the first stage of the DPCG algorithm, the complexity in dividing data space into disjoint grid units, mapping the data points to the data space and counting the number of cell data points is $O(n)$. It is equal to use $O(n)$ time to calculate the local density of each data point (cell). In the second stage, the original DPC algorithm is used to cluster the cells, which seen as data points. It costs $O(m^2)$ time to establish a distance matrix and calculate the local density and the high-density distance. Here, compared to the number of data points n, the number of nonempty grid cells m is very small. So, the speed of running will be significantly faster than the DPC algorithm with the increase of n. Meanwhile, it inherits the advantages of the DPC algorithm, which can detect various kinds of shapes and take simple input parameters and get better clustering performance compared to classical methods (X. Xu et al., 2018).

All these algorithms are implemented and evaluated in the software MATLAB 2014b, and the computer doing experiments is equipped with the Microsoft Windows7 Ultimate System, CPU Intel® Core™i7, and 8.00GB computer memory. The computing time of three clustering algorithms for three fabric samples is shown in Table 2. The computing time of the proposed GPDC algorithm is less than the FCM algorithm and The KFCM algorithm has the largest computing time.

6.3.4 Limitations and Improvements

It is nearly impossible to segment the colour pattern for all kinds of multi-spectral images by the proposed method with constant parameters. There are many factors that can hinder the automatic and accurate colour pixel clustering and colour pattern

segmentation, such as fabric texture, adjacent colours and so on. As shown in Figure 6.12(a), the fabric sample has three adjacent reds which is not easy to separate. Besides, it has small fabric densities and high transmission of light, thereby having the black colour of the holder in the yarn clearances, which make it harder to extract the fabric colours precisely.

The decision graph of the GDPC algorithm is shown in Figure 6.12(b). All potential cluster centers with high distance δ are shown in the decision graph. When the threshold T_δ is set as 7.5 to distinguish the cluster centers and members, the recognized colour pattern is show in Figure 6.12(c). Three adjacent reds are recognized successfully. Unfortunately, one colour indicated by the red arrow in the decision graph of Figure 6.12(b) are not recognized. However, when the threshold T_δ is set as 6.0, this colour can be extracted successfully.

Therefore, we also allow the user to select the cluster centers on the decision graph in our colour pattern recognition system of printed fabrics to guarantee the accuracy and precise. The decision graph can show the colours of all potential clustering centers with high density and their distances from the nearest potential clustering center. Compared with other clustering algorithms, the GDPC algorithm can provide decision graph to realize the interaction of colour center extraction easily and intuitively, which has a better user experience.
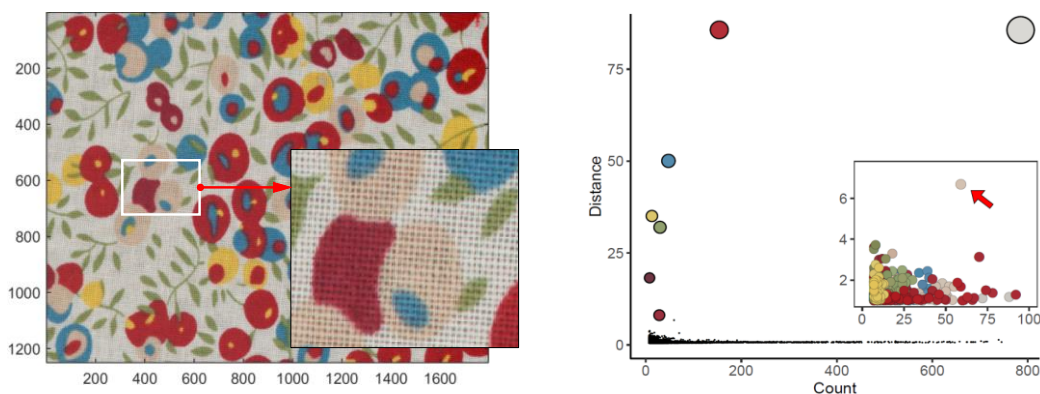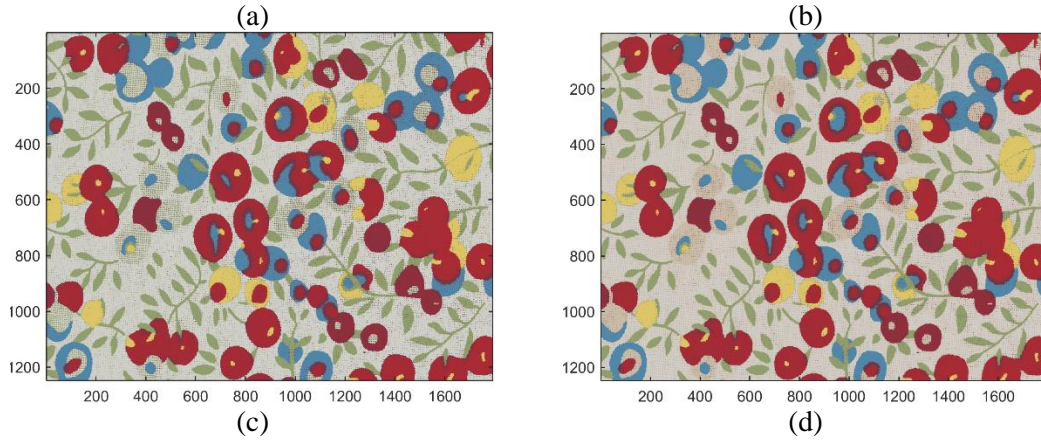
Figure 6.12 Example of user-guided colour extraction. (a) Original fabric sample. (b) Decision graph. (c) Recognized colour pattern with T_δ of 7.5. (d) Recognized colour pattern with T_δ of 6.0.

Besides, deep learning added a huge boost to the already rapid developing field of computer vision. The convolutional neural networks (CNN) have had enormous success on image segmentation problems, such as semantic image segmentation (Badrinarayanan, Kendall, & Cipolla, 2017; Chaurasia & Culurciello, 2017; Lin, Milan, Shen, & Reid, 2017). To obtain a stable and robust CNN, the network must be trained by a large-scale data set of multispectral printed fabric images and the corresponding ground truth of segmented colour patterns. However, a training data set of multispectral printed fabric images may not be always feasible in practical applications and it is difficult to obtain a ground truth of segmented colour patterns in the practical colour segmentation application. Thus, the corresponding colour pattern still need to be recognized manually with the help of the proposed automatic GDPC algorithm and now the solution for this practical application is still limited to unsupervised segmentation algorithms, such as the proposed GDPC algorithm in this article.

6.4 Conclusion

In this chapter, a multispectral imaging system is developed to capture the multispectral fabric image and a grid-based density peaks clustering algorithm is proposed to measure colours of multispectral image of printing fabric. The proposed GDPC algorithm is based on the CIELAB colour values and three reduced features and can be used to colour separation from more intricate multispectral images with higher accuracy and less time consuming, compared with some commonly used colour clustering algorithms, such as FCM and KFCM algorithms. However, there are many other factors that can hinder the automatic and accurate colour pixel clustering and colour pattern segmentation, such as fabric texture, adjacent colours and so on.

Furthermore, the GDPC algorithm can provide decision graph to realize the interaction of colour center extraction easily and intuitively, which has a better user experience, thereby allowing the user to select the cluster centers on the decision graph in our colour pattern recognition system of printed fabrics to guarantee the accuracy and precise.

In the future, we will attempt to collect a sufficient data set of multispectral printed fabric images and use the proposed automatic GDPC algorithm to obtain the corresponding colour patterns combined with the human vision judgment, finally use develop a deep learning method to improve the accuracy of the automatic fabric colour extraction and colour pattern recognition.

Chapter 7 Conclusion and Future Work

7.1 Summary of work

To conclude, this work proposed and experimented computer vision techniques in the fabric image processing with the objectives of having better colour reproduction accuracy and higher efficiency in handling fabric data.

7.1.1 Spectral reflectance reconstruction

An improved reflectance reconstruction method based on L1-norm penalization has been proposed. Using L1-norm, this method can provide the transformation matrix with the favourable sparse property, which can help to achieve better results when measuring the unseen samples. The work verified the proposed method by reconstructing spectral reflection for 4 types of materials (cotton, paper, polyester, and nylon) captured by a multi-spectral imaging system. Each of the materials has its own texture and there are 204 samples in each of the materials / textures in the experiments. Experimental results show that when the texture is not included in the training dataset, L1-norm can achieve better results compared with existing methods using colorimetric measure (i.e., colour difference) and shows consistent accuracy across 4 kinds of materials.

.

7.1.2 Whiteness measurement

The work proposed to use MSI device to measure the whiteness of a flat object which is especially useful for textile and paper production. In order to conduct measurement, a multispectral imaging system is built by integrating with Xenon light and an integral sphere. Different from the ordinary multispectral imaging system for fidelity whiteness

reproduction only for pure reflective materials, this machine can reconstruct the spectral surface for objects which FWAs. To achieve that, the conventional Tungsten is replaced by an Xenon light with integrating sphere. Besides, a UV light box with two filters is designed to simulate two light sources. A linear combination method is extended to combine images under two light sources. At last, a theoretical model is build can applied to whiteness measuring process in the multispectral machine, which ensures the spatial uniformity. The results show the well accuracy and Spatial uniformity for whiteness measurement compared to standard instruments like spectrophotometer.

7.1.3 Knitted fabric classification

In this thesis, a recognition method for knitted fabric structure based on bag of virtual words is proposed. In this work, the common methods in classification for knitted fabric textile are investigated. The KNN classification method cost less time in the experiment. The proposed method shows more accuracy compared to other methods like SVM as classification method and GLCM as feature extraction method.

7.1.4 Printing fabric colour measurement

The proposed GDPC algorithm is based on the CIELAB colour values and three reduced features and can be used to colour separation from more intricate multispectral images with higher accuracy and less time consuming, compared with some commonly used colour clustering algorithms, such as FCM and KFCM algorithms. However, there are many other factors that can hinder the automatic and accurate colour pixel clustering and colour pattern segmentation, such as fabric texture, adjacent colours and so on.

Compared to other methods like FCM, this method show more accuracy and robustly when measuring the colour in printing fabric.

7.2 Future work

The future research work in the development of the multispectral imaging system includes a better light source (e.g., LED) and the extension of different applications using the imaging machine. For example, creating a huge fabric image database for retrieval application.

7.2.1 LED-based multispectral imaging

Traditional multispectral imaging system often uses tungsten halogen lamp or xenon lamp as the illumination source, the disadvantages of these lamps are their high temperature during use and long warm-up time for a stable measurement, especially for certain dyes and pigments on fabrics, which are sensitive to heat and thus causing undesired measurement error. In recent years, the advancement of hight intensity LEDs brings advantages such as low energy consumption (i.e., less heat), fast response time and low cost to multispectral imaging systems. Moreover, LED can be easily controlled using computer programs. These advantages attracted the usage of LED in multispectral imaging systems in many areas.

In contrast to most studies in the literature using an array of LEDs with different colours (e.g., red, green and blue) for illumination, this study uses a single white LED together with a filter wheel mounted with narrow band filters for capturing monochromatic images in different wavelength ranges (i.e., from 400nm to 700nm with 20nm interval). The filter wheel is placed between the lens and the camera in order to filter the light entering the camera. The measured response of the camera is proportional to the

intensity of light entering the sensor. The spectral sensitivity and bias of the system are recovered by a training dataset with known reflectance. The measurement process involves capturing the raw response (data cube) from the monochromic camera with each of the narrow-band filters, performing white balance using pre-defined colours and white or grey board, reflectance reconstruction and whiteness estimation.

7.2.2 Textile image retrieval

Research in Content-Based Image Retrieval (CBIR) systems draws a lot of attention in recent years due to the emergence of large-scale image collections. Instead of being manually annotated by text-based key words, images would be indexed by their own visual content, such as colour, texture and pattern. Many techniques in this research direction have been developed and many image retrieval systems, both research and commercial, have been built sophisticated image processing algorithms have been designed to describe colour, texture, and shape features. Common colour features include colour-covariance matrix, colour histogram, colour moments, and colour coherence vector. MPEG-7 has included dominant colour, colour structure, scalable colour, and colour layout as colour features. Texture features in image retrieval systems include features obtained using Gabor filtering or wavelet transforms. Shape features include aspect ratio, circularity, Fourier descriptors, moment invariants, consecutive boundary segments. There is also a well-known "sematic gap" between the low-level image features with the high-level concepts perceived by humans.

This study plans to develop of a fabric image retrieval system which is based on the techniques of CBIR but with a focus on fabric images which contain fabric-specific features such as yarn colour and weave pattern. A retrieval model serves the purpose of defining the (1) representation of the data and (2) the search mechanism (i.e., the

matching function). Generally, in CBIR, the images are represented as high-dimensional feature vectors. The features can be extracted using colour information, texture information or pattern information contained in the images. For the matching function, usually a distance metric is used such as the Euclidean distance measure or the cosine similarity measure.

One possible future direction is to utilize the structure of the fabric images to perform retrieval because fabric images usually consist of highly repeated and regular structures. The advancement in computer image processing technology enables a higher automation in the textile industry. One of the basic problems during the automation process is to segment the fabric image into meaningful regions. Region segmentation is useful in the design evaluation process, the colour measuring process and also the fabric image retrieval process. More studies in fabric image region segmentation include fuzzy region competition-based methods for fabric design and recolouring, solid-colour and multi-colour region segmentation in yarn-dyed fabric images by constructing statistical models, and automatic layout detection of yarn colours by curve projection methods. Region segmentation can benefit the retrieval performance in fabric image retrieval. It extends the previous works such that clustering of the segmented regions is performed for discovering meaningful patterns in the fabric image.

The objectives of region segmentation are to (1) discover repetitive patterns in yarn-dyed fabric images after region segmentation; and (2) segment the image into different regions where each region contains yarns with identical colours, and then cluster the segmented regions into groups such that each group is coherent in colours. The main challenge in region segmentation is the non-uniformity problem which is caused by the 3D shape of the yarns and results in local pixel-intensity oscillations in individual yarns

when captured by an imaging system. It is proposed to use texture removal technique to solve the non-uniformity problem.

For a brief description of the proposed method, first texture removal using relative total variation technique is performed on the fabric image to obtain the preliminary structure by smoothing out texture edge. Total variation techniques allow the separation of structure from texture in images. Second, Canny edge detection algorithm is used to detect structure edges in the preliminary structure image. Third, a morphological operation is performed on the output of the Canny algorithm to close the gaps between the line segments. After edge detection, the fabric image can be divided into individual segmented regions. The segmented regions are then clustered into groups using their colour information such that regions having similar colours are grouped together. Figure 6.5 shows an example which is the preliminary result of using structure extraction on fabric image.

7.2.3 Deep Learning

In our current work, hand-crafted low-level image features such as SIFT and SURF models are used to represent the images. However, there is a well-known "sematic gap" between the low-level image pixels captured by machines (and represented by those low-level features) and the high-level sematic concept perceived by humans. The "sematic gap" represents the root challenge in the field of artificial intelligence studying methods of building intelligent machines to perform human-like tasks. Deep learning, a branch of machine learning, is one of the promising techniques to address this root challenge.

Deep leaning, which uses a family of machine learning algorithms to model high-level abstractions from the data, employs a deep architecture with multiple layers of non-

linear transformations. Using the multiple layers of transformations, deep learning algorithms simulates the human brain to learn features at difference level of abstractions automatically, it allows a computer program to learn complex functions without the hand-crafted features with specific domain knowledge such e.g., SIFT and SURF features.

Deep learning draws tremendous attention recently in various fields which include speech recognition, object recognition, natural language processing and image retrieval. Researchers have used deep learning algorithms for almost every computer vision tasks and it is worth to investigate the use of deep learning in fabric image retrieval.

References

AATCC, T. (2018). AATCC Test Method 110-2015, Whiteness of textiles. *American Association of Textile Chemists and Colorists, Durham}*, 185--186.

Aman, Z. (2012). *Efficiency of Fluorescent Whitening Agents in Pigment Coatings*.

Badrinarayanan, V., Kendall, A., & Cipolla, R. (2017). Segnet: A deep convolutional encoder-decoder architecture for image segmentation. *IEEE Transactions on Pattern Analysis and Machine Intelligence, 39*(12), 2481-2495.

Bay, H., Tuytelaars, T., & Van Gool, L. (2006). *Surf: Speeded up robust features.* Paper presented at the European conference on computer vision.

Bezdek, J. C. (2013). *Pattern recognition with fuzzy objective function algorithms*: Springer Science & Business Media.

Bishop, C. M. (2006). *Pattern recognition and machine learning*: springer.

Boyd, S., Parikh, N., & Chu, E. (2011). *Distributed optimization and statistical learning via the alternating direction method of multipliers*: Now Publishers Inc.

Brauers, J., & Aach, T. (2011). Geometric calibration of lens and filter distortions for multispectral filter-wheel cameras. *IEEE Transactions on Image Processing, 20*(2), 496-505.

Brauers, J., & Aach, T. J. I. T. o. I. P. (2010). Geometric calibration of lens and filter distortions for multispectral filter-wheel cameras. *20*(2), 496-505.

Brauers, J., Schulte, N., & Aach, T. J. I. t. o. i. p. (2008). Multispectral filter-wheel cameras: Geometric distortion model and compensation algorithms. *17*(12), 2368-2380.

Can Karaimer, H., & Brown, M. S. (2018). *Improving color reproduction accuracy on cameras.* Paper presented at the Proceedings of the IEEE Conference on Computer Vision and Pattern Recognition.

Chang, C.-H., Xu, P., Xiao, R., & Srikanthan, T. (2005). New adaptive color quantization method based on self-organizing maps. *IEEE transactions on neural networks, 16*(1), 237-249.

Chaurasia, A., & Culurciello, E. (2017). *Linknet: Exploiting encoder representations for efficient semantic segmentation.* Paper presented at the 2017 IEEE Visual Communications and Image Processing (VCIP).

Chen, S.-J., Shen, H.-L., Li, C., & Xin, J. H. J. I. T. o. I. P. (2017). Normalized total gradient: A new measure for multispectral image registration. *27*(3), 1297-1310.

Chen, S.-J., & Shen, H.-L. J. I. T. o. I. P. (2015). Multispectral image out-of-focus deblurring using interchannel correlation. *24*(11), 4433-4445.

Cheng, Q., Liu, Z., Huang, J., & Cheng, G. (2016). Community detection in hypernetwork via Density-Ordered Tree partition. *Applied Mathematics and Computation, 276*, 384-393.

Coppel, L. G., Andersson, M., Neuman, M., & Edström, P. (2012). Fluorescence model for multi-layer papers using conventional spectrophotometers. *Nordic Pulp Paper Research Journal, 27*(2), 418-425.

Csurka, G., Dance, C., Fan, L., Willamowski, J., & Bray, C. (2004). *Visual categorization with bags of keypoints.* Paper presented at the Workshop on statistical learning in computer vision, ECCV.

Fu, Y., Lam, A., Kobashi, Y., Sato, I., Okabe, T., Sato, Y., & Ieee. (2014). Reflectance and Fluorescent Spectra Recovery based on Fluorescent Chromaticity Invariance under Varying Illumination. In *2014 Ieee Conference on Computer Vision and Pattern Recognition* (pp. 2171-2178). New York: Ieee.

Fu, Y., Lam, A., Matsushita, Y., Sato, I., & Sato, Y. (2014). Interreflection Removal Using Fluorescence. *Computer Vision - Eccv 2014, Pt V, 8693*, 203-217.

Fu, Y., Lam, A., Sato, I., Okabe, T., & Sato, Y. (2013). *Separating reflective and fluorescent components using high frequency illumination in the spectral domain.* Paper presented at the Proceedings of the IEEE International Conference on Computer Vision.

Fu, Y., Lam, A., Sato, I., Okabe, T., Sato, Y., & Ieee. (2013). Separating Reflective and Fluorescent Components Using High Frequency Illumination in the Spectral Domain. In *2013 Ieee International Conference on Computer Vision* (pp. 457-464). New York: Ieee.

Fu, Y., Zheng, Y. R., Zhang, L., & Huang, H. (2018). Spectral Reflectance Recovery From a Single RGB Image. *Ieee Transactions on Computational Imaging, 4*(3), 382-394. doi:10.1109/tci.2018.2855445

Gärtner, F., & Griesser, R. (1975). Eine Vorrichtung zur Messung von optischen Aufhellern mit konstanter UV-Anregung. *Die Farbe, 24*, 199-207.

Gay, J., Melo, C., & Hirschler, R. (2004). *Instrumental whiteness evaluation: Practical results of inter-instrument agreement tests.* Paper presented at the Interim Meeting of the International Color Association, Proceedings (AIC Color and Paints).

Guo, L., Lin, J.-H., Guo, Q., & Liu, J.-G. (2016). Identifying multiple influential spreaders in term of the distance-based coloring. *Physics Letters A, 380*(7-8), 837-842.

Hardeberg, J. Y. (2001). *Acquisition and reproduction of color images: colorimetric and multispectral approaches*: Universal-Publishers.

Hardeberg, J. Y., Schmitt, F., & Brettel, H. (2002). Multispectral color image capture using a liquid crystal tunable filter. *Optical engineering, 41*(10), 2532-2548. doi:10.1117/1.1503346

Hastie, T., & Tibshirani, R. (1996). Discriminant adaptive nearest neighbor classification. *IEEE Transactions on Pattern Analysis and Machine Intelligence, 18*(6), 607-616. doi:10.1109/34.506411

Heikkinen, V., Jetsu, T., Parkkinen, J., Hauta-Kasari, M., Jaaskelainen, T., & Lee, S. D. (2007). Regularized learning framework in the estimation of reflectance spectra from camera responses. *J Opt Soc Am A Opt Image Sci Vis, 24*(9), 2673-2683. doi:10.1364/josaa.24.002673

Heikkinen, V., Jetsu, T., Parkkinen, J., Hauta-Kasari, M., Jaaskelainen, T., & Lee, S. D. J. J. A. (2007). Regularized learning framework in the estimation of reflectance spectra from camera responses. *24*(9), 2673-2683.

Heikkinen, V., Lenz, R., Jetsu, T., Parkkinen, J., Hauta-Kasari, M., & Jaaskelainen, T. (2008). Evaluation and unification of some methods for estimating reflectance spectra from RGB images. *Journal of the Optical Society of America a-Optics Image Science and Vision, 25*(10), 2444-2458. doi:Doi 10.1364/Josaa.25.002444

Herzog, P. G., & Hill, B. (2003). *Multispectral imaging and its applications in the textile industry and related fields.* Paper presented at the PICS.

Hirai, K., Osawa, N., Hori, M., Horiuchi, T., & Tominaga, S. (2018). High-dynamic-range spectral imaging system for omnidirectional scene capture. *Journal of Imaging, 4*(4), 53.

Imura, K., Imai, K., Kawabata, T., & Makino, M. (1997). Measuring apparatus for measuring an optical property of a fluorescent sample. In: Google Patents.

Jafari, R., & Amirshahi, S. H. J. T. R. J. (2007). A comparison of the CIE and Uchida whiteness formulae as predictor of average visual whiteness evaluation of textiles. *77*(10), 756-763.

Jiang, J., & Gu, J. (2012). *Recovering spectral reflectance under commonly available lighting conditions.* Paper presented at the 2012 IEEE Computer Society Conference on Computer Vision and Pattern Recognition Workshops.

Kanjanawanishkul, K., & Uyyanonvara, B. (2005). Novel fast color reduction algorithm for time-constrained applications. *Journal of Visual Communication and Image Representation, 16*(3), 311-332.

Kuo, C.-F. J., & Kao, C.-Y. (2008). Automatic color separating system for printed fabric using the self-organizing map network approach. *Fibers and Polymers, 9*(6), 708-714.

Kuo, C.-F. J., & Shih, C.-Y. (2011). Printed fabric computerized automatic color separating system. *Textile Research Journal, 81*(7), 706-713.

Kuo, C. F. J., & Kao, C. Y. (2007). Self-organizing map network for automatically recognizing color texture fabric nature. *Fibers and Polymers, 8*(2), 174-180.

Kuo, C. F. J., Kao, C. Y., & Chiu, C. H. (2009). Integrating a Genetic Algorithm and a Self-organizing Map Network for an Automatically Separating Color Printed Fabric System. *Textile Research Journal, 79*(13), 1235-1244. doi:10.1177/0040517509102386

Kuo, C. F. J., Shih, C. Y., Kao, C. Y., & Lee, J. Y. (2005). Color and pattern analysis of printed fabric by an unsupervised clustering method. *Textile Research Journal, 75*(1), 9-12. doi:10.1177/004051750507500103

Kuo, C. F. J., Shih, C. Y., & Lee, J. Y. (2004). Automatic recognition of fabric weave patterns by a fuzzy C-means clustering method. *Textile Research Journal, 74*(2), 107-111.

Kuo, C. F. J., Shih, C. Y., & Lee, J. Y. (2008). Separating color and identifying repeat pattern through the automatic computerized analysis system for printed fabrics. *Journal of Information Science and Engineering, 24*(2), 453-467.

Li, J., Wang, W., Deng, N., & Xin, B. (2020). A novel digital method for weave pattern recognition based on photometric differential analysis. *Measurement, 152*, 107336. doi:10.1016/j.measurement.2019.107336

Lin, G., Milan, A., Shen, C., & Reid, I. (2017). *Refinenet: Multi-path refinement networks for high-resolution semantic segmentation.* Paper presented at the Proceedings of the IEEE conference on computer vision and pattern recognition.

Liu, J. H., Jiang, H. X., Liu, X., & Chai, Z. (2014). Automatic measurement for dimensional changes of woven fabrics based on texture. *Measurement Science and Technology, 25*(1). doi:Artn 015602

10.1088/0957-0233/25/1/015602

Lowe, D. G. (2004). Distinctive image features from scale-invariant keypoints. *International journal of computer vision, 60*(2), 91-110. doi:Doi 10.1023/B:Visi.0000029664.99615.94

Luo, L., Shao, S. J., Shen, H. L., & Xin, J. H. (2013). An unsupervised method for dominant colour region segmentation in yarn-dyed fabrics. *Coloration Technology, 129*(6), 389-397. doi:10.1111/cote.12063

Luo, L., Shen, H. L., Shao, S. J., & Xin, J. (2015a). Empirical model for matching spectrophotometric reflectance of yarn windings and multispectral imaging reflectance of single strands of yarns. *J Opt Soc Am A Opt Image Sci Vis, 32*(8), 1459-1467. doi:10.1364/JOSAA.32.001459

Luo, L., Shen, H. L., Shao, S. J., & Xin, J. H. (2015b). An efficient method for solid-colour and multicolour region segmentation in real yarn-dyed fabric images. *Coloration Technology, 131*(2), 120-130. doi:10.1111/cote.12131

Luo, L., Shen, H. L., Shao, S. J., & Xin, J. H. (2015c). A multispectral imaging approach to colour measurement and colour matching of single yarns without winding. *Coloration Technology, 131*(4), 342-351. doi:10.1111/cote.12162

Luo, L., Shen, H. L., Shao, S. J., & Xin, J. H. (2016). Colour matching comparison between spectrophotometric and multispectral imaging measurements. *Coloration Technology, 132*(1), 17-27. doi:10.1111/cote.12191

Lv, T. J., & Long, H. R. (2015). Feature matching of fancy weft knitted stitch based on modified SURF algorithm. *Textile Research Journal, 85*(7), 751-758. doi:10.1177/0040517514551465

Martínez-Domingo, M. Á., Valero, E. M., Hernández-Andrés, J., Tominaga, S., Horiuchi, T., & Hirai, K. J. O. e. (2017). Image processing pipeline for segmentation and material classification based on multispectral high dynamic range polarimetric images. *25*(24), 30073-30090.

McDonald, R. (1997). *Colour physics for industry*: The Society of Dyers and Colourists.

Mingoti, S. A., & Lima, J. O. (2006). Comparing SOM neural network with Fuzzy c-means, K-means and traditional hierarchical clustering algorithms. *European journal of operational research, 174*(3), 1742-1759.

Mo, H., Xu, B., Ouyang, W., & Wang, J. (2017). Color segmentation of multi-colored fabrics using self-organizing-map based clustering algorithm. *Textile Research Journal, 87*(3), 369-380.

Mosny, M., & Funt, B. (2006). *Multispectral colour constancy.* Paper presented at the Color and Imaging Conference.

Murakami, Y., Obi, T., Yamaguchi, M., Ohyama, N., & Komiya, Y. (2001). Spectral reflectance estimation from multi-band image using color chart. *Optics Communications, 188*(1-4), 47-54. doi:Doi 10.1016/S0030-4018(00)01131-7

Murakami, Y., Obi, T., Yamaguchi, M., Ohyama, N., & Komiya, Y. J. O. c. (2001). Spectral reflectance estimation from multi-band image using color chart. *188*(1-4), 47-54.

Ng, A. Y., Jordan, M. I., & Weiss, Y. (2002). *On spectral clustering: Analysis and an algorithm.* Paper presented at the Advances in neural information processing systems.

Nowak, E., Jurie, F., & Triggs, B. (2006). *Sampling strategies for bag-of-features image classification.* Paper presented at the European conference on computer vision.

Nyström, D. (2006). *Colorimetric and multispectral image acquisition.* Institutionen för teknik och naturvetenskap,

Okawa, H., Shimano, M., Asano, Y., Bise, R., Nishino, K., & Sato, I. (2019). Estimation of Wetness and Color From A Single Multispectral Image. *IEEE transactions on pattern analysis machine intelligence*.

Oliva, A., & Torralba, A. (2001). Modeling the shape of the scene: A holistic representation of the spatial envelope. *International journal of computer vision, 42*(3), 145-175. doi:Doi 10.1023/A:1011139631724

Ouyang, W., Xu, B., & Yuan, X. (2019). Color segmentation in multicolor images using node-growing self-organizing map. *Color Research & Application, 44*(2), 184-193.

Pan, R., Gao, W., Liu, J., Wang, H. J. F., & Europe, T. i. E. (2010). Automatic inspection of woven fabric density of solid colour fabric density by the Hough transform. *18*(4), 81.

Pointer, M. (1981). A comparison of the CIE 1976 colour spaces. *Color Research & Application, 6*(2), 108-118.

Puebla, C. (2006a). Whiteness assessment: A primer. *Axiphos GmbH, Germany, 18*.

Puebla, C. (2006b). Whiteness assessment: A primer. *Concepts, Determination and Control of Perceived Whiteness. Axiphos GmbH. Internet: www. axiphos. com/WhitenessPrimer. pdf (2.02. 2007)*.

Raheja, J. L., Kumar, S., & Chaudhary, A. (2013). Fabric defect detection based on GLCM and Gabor filter: A comparison. *Optik, 124*(23), 6469-6474. doi:10.1016/j.ijleo.2013.05.004

Rodarmel, C., & Shan, J. (2002). Principal component analysis for hyperspectral image classification. *Surveying and Land Information Science, 62*(2), 115-122.

Rodriguez, A., & Laio, A. (2014). Clustering by fast search and find of density peaks. *Science, 344*(6191), 1492-1496.

Sato, I., Okabe, T., & Sato, Y. (2012). *Bispectral photometric stereo based on fluorescence.* Paper presented at the Computer Vision and Pattern Recognition (CVPR), 2012 IEEE Conference on.

Schanda, J. (2007). *Colorimetry: understanding the CIE system*: John Wiley & Sons.

Schneider, D., Gloy, Y. S., & Merhof, D. (2014). Vision-Based On-Loom Measurement of Yarn Densities in Woven Fabrics. *IEEE transactions on instrumentation and measurement, 64*(4), 1063-1074.

Scholkopf, B., & Smola, A. J. (2001). *Learning with kernels: support vector machines, regularization, optimization, and beyond*: MIT press.

Shen, H. L., Cai, P. Q., Shao, S. J., & Xin, J. H. (2007). Reflectance reconstruction for multispectral imaging by adaptive Wiener estimation. *Opt Express, 15*(23), 15545-15554. doi:10.1364/oe.15.015545

Shen, H. L., Xin, J. H., & Shao, S. J. (2007). Improved reflectance reconstruction for multispectral imaging by combining different techniques. *Opt Express, 15*(9), 5531-5536. doi:10.1364/oe.15.005531

Shimano, M., Okawa, H., Asano, Y., Bise, R., Nishino, K., & Sato, I. (2017). *Wetness and color from a single multispectral image.* Paper presented at the Proceedings of the IEEE Conference on Computer Vision and Pattern Recognition.

Shimano, N. J. I. T. o. I. P. (2006). Recovery of spectral reflectances of objects being imaged without prior knowledge. *15*(7), 1848-1856.

Shiradkar, R., Shen, L., Landon, G., Heng Ong, S., & Tan, P. (2014). *A new perspective on material classification and ink identification.* Paper presented at the Proceedings of the IEEE Conference on Computer Vision and Pattern Recognition.

Shrestha, R., & Hardeberg, J. Y. (2014). *Evaluation and comparison of multispectral imaging systems.* Paper presented at the Color and Imaging Conference.

Sivic, J., & Zisserman, A. (2008). Efficient visual search of videos cast as text retrieval. *IEEE transactions on pattern analysis and machine intelligence, 31*(4), 591-606.

Sumner, R. (2014). Processing raw images in matlab.

Tominaga, S., Hirai, K., & Horiuchi, T. (2018a). *Appearance reconstruction of 3D fluorescent objects under different conditions.* Paper presented at the Color and Imaging Conference.

Tominaga, S., Hirai, K., & Horiuchi, T. (2018b). Estimation of fluorescent Donaldson matrices using a spectral imaging system. *Optics express, 26*(2), 2132-2148.

Tominaga, S., Hirai, K., & Horiuchi, T. (2019). *Appearance Reconstruction of Fluorescent Objects Based on Reference Geometric Factors.* Paper presented at the Color and Imaging Conference.

Tominaga, S., & Okajima, R. (2000). *Object recognition by multi-spectral imaging with a liquid crystal filter.* Paper presented at the Proceedings 15th International Conference on Pattern Recognition. ICPR-2000.

Uchida, H. (1998). A new whiteness formula. *Color Research and Application, 23*(4), 202-209.

Vik, M., Viková, M., & Periyasamy, A. P. (2015). *Influence of SPD on Whiteness value of FWA treated samples.* Paper presented at the 21st International Conference LIGHT SVĚTLO.

Wang, X., Georganas, N. D., & Petriu, E. M. (2011). Fabric Texture Analysis Using Computer Vision Techniques. *Ieee Transactions on Instrumentation and Measurement, 60*(1), 44-56. doi:10.1109/tim.2010.2069850

Westland, S., Ripamonti, C., & Cheung, V. (2012). *Computational colour science using MATLAB*: John Wiley & Sons.

Xiao, Y., & Yu, J. (2012). Partitive clustering (K-means family). *Wiley Interdisciplinary Reviews-Data Mining and Knowledge Discovery, 2*(3), 209-225. doi:10.1002/widm.1049

Xin, B. J., Hu, J. L., Baciu, G., & Yu, X. B. (2009). Investigation on the Classification of Weave Pattern Based on an Active Grid Model. *Textile Research Journal, 79*(12), 1123-1134. doi:10.1177/0040517508101459

Xin, J. H., Shen, H.-l., & Ge, Q.-g. (2020a). Color quality assessment based on multispectral imaging. In: Google Patents.

Xin, J. H., Shen, H.-l., & Ge, Q.-g. (2020b). Multispectral color imaging device based on integrating sphere lighting and calibration methods thereof. In: Google Patents.

Xu, B. G. (1996). Identifying fabric structures with Fast Fourier Transform techniques. *Textile Research Journal, 66*(8), 496-506.

Xu, X., Ding, S., Du, M., & Xue, Y. (2018). DPCG: an efficient density peaks clustering algorithm based on grid. *International Journal of Machine Learning and Cybernetics*, 1-12.

Yang, L. (2017). Detailed analysis of the UV-adjustment techniques used in paper and graphic industries. *Color Research and Application, 42*(1), 19-26.

Zhang, C., & Sato, I. (2013). Image-based separation of reflective and fluorescent components using illumination variant and invariant color. *IEEE transactions on pattern analysis and machine intelligence, 35*(12), 2866-2877.

Zhang, D.-Q., & Chen, S.-C. (2003). Clustering incomplete data using kernel-based fuzzy c-means algorithm. *Neural processing letters, 18*(3), 155-162.

Zhang, J., Wang, J. A., Pan, R. R., Zhou, J., & Gao, W. D. (2018). A computer vision-based system for automatic detection of misarranged warp yarns in yarn-dyed fabric. Part I: continuous segmentation of warp yarns. *Journal of the Textile Institute, 109*(5), 577-584. doi:10.1080/00405000.2017.1361580

Zhang, J., Xin, B. J., & Wu, X. J. (2014). Density measurement of yarn dyed woven fabrics based on dual-side scanning and the FFT technique. *Measurement Science and Technology, 25*(11), 0957-0233. doi:Artn 115007

10.1088/0957-0233/25/11/115007

Zhang, X., & Xu, H. (2008). Reconstructing spectral reflectance by dividing spectral space and extending the principal components in principal component analysis. *J Opt Soc Am A Opt Image Sci Vis, 25*(2), 371-378. doi:10.1364/josaa.25.000371

Zheng, Y., Sato, I., & Sato, Y. (2014). *Spectra estimation of fluorescent and reflective scenes by using ordinary illuminants.* Paper presented at the European Conference on Computer Vision.

Zhu, D. D., Pan, R. R., Gao, W. D., & Zhang, J. (2015). Yarn-Dyed Fabric Defect Detection Based on Autocorrelation Function and Glcm. *Autex Research Journal, 15*(3), 226-232. doi:10.1515/aut-2015-0001